PHYSICAL REVIEW B VOLUME 16, NUMBER 11 1 DECEMBER 1977

Electronic structure of ferromagnetic hcp cobalt. I. Band properties*

C. M. Singal and T. P. Das
Department of Physics, State University of New York, Albany, New York 12222
(Received 12 December 1974; revised manuscript received 17 June 1975)

A first-principles self-consistent, unrestricted Hartree-Fock, hybridized-tight-binding-plane-wave, electronic-structure calculation for ferromagnetic cobalt in hexagonal-close-packed structure is presented. The nonlocal Hartree-Fock exchange-interaction matrix elements were explicitly included in the Hamiltonian matrix and correlation effects on the one-electron energy levels were incorporated through the pair correlation energies among the core, $3d$, and conduction electrons. The most important correlation effect was that associated with the $3d$-band electrons and this was included through the Hubbard-Kanamori bandwidth-dependent model. Self-consistency was reached through an iterative procedure with respect to the density matrix, bandwidth, and the magnetic moment. For the latter, we obtained a value of $1.58\mu_B$ as compared to the experimental value of $1.56\mu_B$. We have utilized the results of our energy-band calculations to study different energy- and wave-function-related properties, namely, the work function, electronic density of states, bandwidth and exchange splittings, specific heat, Fermi-surface cross sections, and spin-wave spectra, results for which are presented here and comparisons made with experiment. Our results for a number of other properties will be presented in subsequent papers.

I. INTRODUCTION

The first-principles understanding of the electronic structure of ferromagnetic metals has become a subject of considerable interest in recent years. This interest has been generated as a consequence of parallel developments in refined theoretical techniques[1-5] for studying electronic wave functions and energy bands and the development of sophisticated experimental techniques to study a variety of properties. Among these are the shape and dimensions of the Fermi surface,[6-8] by de Haas–van Alphen and related measurements, the density of states through ultraviolet photoemission techniques,[9] the spin splittings of core levels by x-ray photoemission techniques[10,11] (ESCA), the magnetization through neutron-scattering[12] techniques, and the hyperfine fields[13-16] by nuclear magnetic resonance and Mössbauer techniques in both the pure metals and a variety of alloys.[16] Among the theoretical techniques that have been employed are the augmented plane wave[4,5] and Kohn, Korringa, and Rostoker[2] procedures, the tight-binding[3] procedure with extensive basis states, and the hybridized tight-binding-orthogonalized-plane-wave (OPW)[1] procedure. Calculations based on the first three procedures[2-5] have made use of a local $\vec{r}$-dependent potential approximation for the exchange interaction, while the last procedure[1] has utilized the actual nonlocal Hartree-Fock (HF) matrix elements involving the $1/r_{12}$ explicitly. This feature is particularly important for the study of magnetic hyperfine fields.[1,17] An additional feature of this last procedure, which is a consequence of using the actual HF exchange, is that the correlation effects can be introduced explicitly since they are completely absent in the one-electron HF approximation. In our present investigations on ferromagnetic cobalt, we have mainly followed this last procedure, which had been applied earlier to ferromagnetic iron,[1] with some modifications. One of these is aimed at substantially reducing the computational effort in the calculation of two-center Coulomb and exchange interactions, without sacrificing any accuracy, thereby making it practicable to attempt some cycles of self-consistency. Other modifications involve the incorporation of correlation effects in core states and of the perturbation of core-state energies and wave functions in the metal with respect to those for the free atom. In our investigations on ferromagnetic cobalt, we have studied all the properties mentioned before, as well as a number of additional ones. The results of these investigations will be published in a series of articles. In the present article we shall describe the procedure for the band calculation and discuss and compare with experiment, both the magnetic moment obtained self-consistently[12] and a number of Fermi-surface and band properties, such as Fermi-surface cross sections[6-8] in different directions, the total density-of-states curve,[9] and individual density of states for the majority- and minority-spin states and the work function.[18]

In Sec. II, first a brief review of HF theory as applied to metals is presented and some of the important notations to be used in this work are introduced together with the choice of the variational basis set for the hybridized tight-binding–OPW procedure that we have employed to permit suffi-

cient flexibility for adequate representation of both the $3d$-like and freelike band wave functions. This section also includes a description of the method of evaluation of Hamiltonian matrix elements, particularly the Coulomb and exchange matrix elements, and especially the multicenter contributions to these matrix elements. Section III will deal with the incorporation of correlation effects for core, $3d$-like, and freelike electrons by appropriate procedures.[19-22] In Sec. IV we first discuss the self-consistency of the band calculation with respect to the magnetization and $3d$-like and freelike band populations. Sec. V presents the band structure and analyzes several specific features of the bands, for example, their crystal-field-like splittings, spin splittings, the $\vec{k}$ dependence of these splittings and the extent of hybridization between OPW and $3d$ characters in the energy bands. This section will also deal with our results on the magnetic moment, the work function, the density-of-states curve, and Fermi-surface cross sections and comparisons with corresponding experimental data and results of earlier theoretical investigations. Section VI presents concluding remarks together with suggestions for possible modifications to further improve agreement with experiment.

II. DESCRIPTION OF HARTREE-FOCK PROCEDURE FOR METALS

In this section, we shall review the Hartree-Fock theory as applied to metals and briefly discuss the choice of basis sets and evaluation of Coulomb and exchange integrals. A more detailed description of the procedure, together with useful technical points, is available elsewhere.[23]

A. Hartree-Fock formalism and choice of basis states

The HF Hamiltonian is a one-electron Hamiltonian derived from the more complete Hamiltonian

$$H=-\frac{\hbar^2}{2m}\sum_i \nabla_i^2-\sum_{i,l}\zeta_l\frac{e^2}{|\vec{r}_i-\vec{R}_l|}+\frac{1}{2}\sum_{i\neq j}\frac{e^2}{|\vec{r}_i-\vec{r}_j|}, \tag{2.1}$$

where ζ_l is the nuclear charge at the atomic site $\vec{R}_l$ and $\vec{r}_i$ is the coordinate for the electron. In the one-electron HF approximation, each electron moves in the average potential from the other electrons and the antisymmetrized wave function Ψ of N electrons is a Slater determinant of their spin orbitals u_i. While one can always derive Hartree-Fock equations[24] for u_i, one can obtain their solutions[25,26] conveniently through numerical solution of appropriate differential equations, only for atomic systems because of the spherical symmetry of their Hartree-Fock potential. For molecules and solid state one has to adopt a variational procedure to solve the Hartree-Fock equations. Thus the spin-orbital u_i is expanded in a set of known linearly independent basis functions ϕ_n with the total number of functions N' greater than N.

$$u_i=\sum_n C_{ni}\phi_n . \tag{2.2}$$

On taking the expectation value of the Hamiltonian in Eq. (2.1) over the determinantal wave function Ψ built from the one-electron spin-orbitals u_i and minimizing with respect to variations in the variation parameters C_{ni}, we get the usual set of linear equations for C_{ni} which lead to the secular equation of dimension N':

$$\det|H_{mn}-ES_{mn}|=0, \tag{2.3}$$

where

$$S_{mn}=\langle\phi_m|\phi_n\rangle \tag{2.4}$$

and

$$H_{mn}=I_{mn}+J_{mn}+K_{mn}, \tag{2.5}$$

where

$$I_{mn}=-\frac{\hbar^2}{2m}\langle\phi_m(1)|\nabla_1^2|\phi_n(1)\rangle-\sum_l \zeta e^2\langle\phi_m(1)|\frac{1}{|\vec{r}_1-\vec{R}_l|}|\phi_n(1)\rangle,$$

$$J_{mn}=\sum_j\langle\phi_m(1)u_j(2)|\frac{e^2}{r_{12}}|\phi_n(1)u_j(2)\rangle, \tag{2.6}$$

and

$$K_{mn}=-\sum_j\langle\phi_m(1)u_j(2)|\frac{e^2}{r_{12}}|u_j(1)\phi_n(2)\rangle .$$

S_{mn} representing elements of the overlap matrix and H_{mn} elements of the HF Hamiltonian matrix, the I_{mn}, J_{mn}, and K_{mn} being, respectively, the one-electron, Coulomb, and exchange contributions to H_{mn}. On solving Eq. (2.3), we get the energy eigenvalues ε_i, for which the corresponding eigenfunctions u_i can be obtained by determining the C_{ni} from the equations:

$$\sum_n (H_{mn}-\varepsilon_i S_{mn})C_{ni}=0 \tag{2.7}$$

combined with the normalization condition:

$$\sum_{m,n} C_{mi}^* S_{mn} C_{ni}=1 . \tag{2.8}$$

Since the matrix elements in the overlap and Hamiltonian matrix in Eqs. (2.4) and (2.5) involve integration over spin components of the basis functions as well, it is clear that H_{mn} and S_{mn} will be zero if ϕ_m and ϕ_n have orthogonal spins. Consequently, each of the H and S matrices and the secular determinant can be decomposed into two separate square blocks for the spin-up and spin-down directions. This corresponds to the unrestricted-Hartree-Fock approximation[27] which is employed here.

The plane-wave (PW) and tight-binding functions which are utilized here as basis functions in constructing the one electron eigenfunctions are defined as follows for our hcp lattice.

$$\phi^{\mathrm{PW}}_{\vec{k}+\vec{K}} = (2N\Omega)^{-1/2} e^{i(\vec{k}+\vec{K})\cdot\vec{r}} \tag{2.9}$$

and

$$\phi^{(\vec{r})}_{nlmp,\vec{k}} = (2N)^{-1/2} \sum_j \left[e^{i\vec{k}\cdot(\vec{R}_j - \vec{\rho}/2)} \phi_{nlm}(\vec{r} - \vec{R}_j + \tfrac{1}{2}\vec{\rho}) + p e^{i\vec{k}\cdot(\vec{R}_j + \vec{\rho}/2)} \phi_{nlm}(\vec{r} - \vec{R}_j - \tfrac{1}{2}\vec{\rho}) \right]. \tag{2.10}$$

Here

$$p = \pm 1 \tag{2.11}$$

and

$$\vec{\rho} = \tfrac{1}{2}\vec{t}_1 + \tfrac{1}{3}\vec{t}_2 + \tfrac{2}{3}\vec{t}_3 \tag{2.12}$$

represents the vector joining one atom in the hcp unit cell (Fig. 1) to the other atom, the origin being taken at the midpoint of such a vector, with $\vec{t}_1$, $\vec{t}_2$, and $\vec{t}_3$ representing primitive lattice vectors for the hcp structure. The presence of two atoms in the unit cell leads to a multiplicity of two in the tight-binding functions. Our calculations were performed for the lattice parameters a and c of the cobalt hcp structure appropriate[28] for 0°K, namely

$$a = 2.5007\ \text{Å} = 4.725\,80\ \text{a.u.},$$
$$c = 4.055\,72\ \text{Å} = 7.664\,37\ \text{au.}. \tag{2.13}$$

We shall thus obtain the band-structure appropriate to 0°K, which is appropriate for most of the experimental data we plan to interpret.

The form of the one-electron variational function, which we have chosen and which is simultaneously suitable for core electrons, valence electrons ($3d$-like electrons) and conduction electrons (freelike electrons) can be referred to as the hybridized tight-binding-plane-wave wave function:

$$\psi_{\vec{k}t\sigma}(\vec{r}) = \Big(\sum_{\vec{K}} C_{\vec{k}t\sigma,\vec{K}} \phi^{\mathrm{PW}}_{\vec{k}+\vec{K}}(\vec{r}) + \sum_{nlmp} C_{\vec{k}t\sigma,nlmp} \phi_{nlmp,\vec{k}}(\vec{r}) \Big) \begin{pmatrix} \alpha \\ \beta \end{pmatrix}_\sigma \tag{2.14}$$

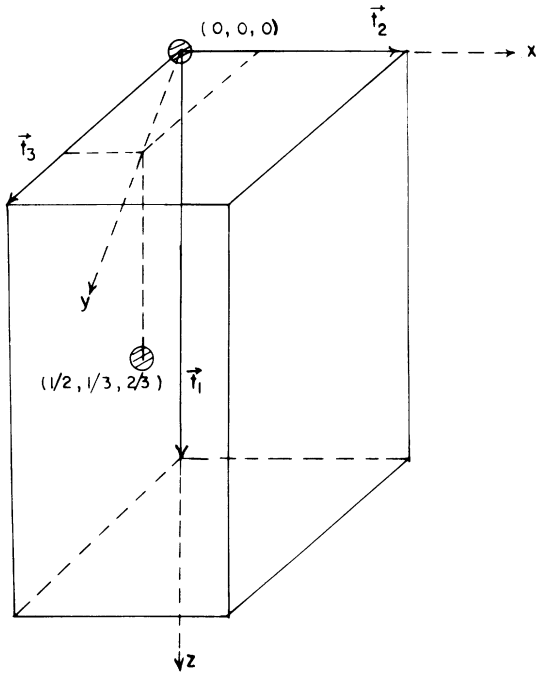

FIG. 1. Direct lattice unit cell hcp structure.

the summations in nlm running over the core and $3d$ states. For core states, the coefficients of the plane-wave components will be negligible. For freelike electrons, the relative coefficients of the core and $3d$ functions will be close to those for a linear combination of orthogonalized plane-wave (OPW) functions,[29] while for $3d$-like eigenfunctions in the metal, the coefficients of the $3d$ tight-binding wave functions are expected to predominate. The plane-wave components in the latter case can be appreciable owing to the mixing or hybridization caused by the potential and from the influence of interatomic overlaps. Correspondingly for freelike electrons, the eigenfunction $\psi_{\vec{k}t\sigma}$ can be expressed as a linear combination of OPW functions and finite admixtures of $3d$ tight-binding functions due to hybridization effects.

From earlier paramagnetic band-structure calculations[2] in cobalt, it has been found that the number of $3d$-like electrons in the metal is about one more than that in the free atom in common with the situation in iron metal.[1] In free cobalt atom (apart from configuration mixing due to correlation effects) the ground state is $3d^7 4s^2(^4F)$. Since cobalt metal seems to lead to a configuration close to $3d^8 4s^1$, it is desirable to obtain the wave functions for all the core and $3d$ and $4s$ states for this configuration by solving the appropriate Hartree-Fock equations. However, since most of the magnetization is due to the $3d$-like electrons,

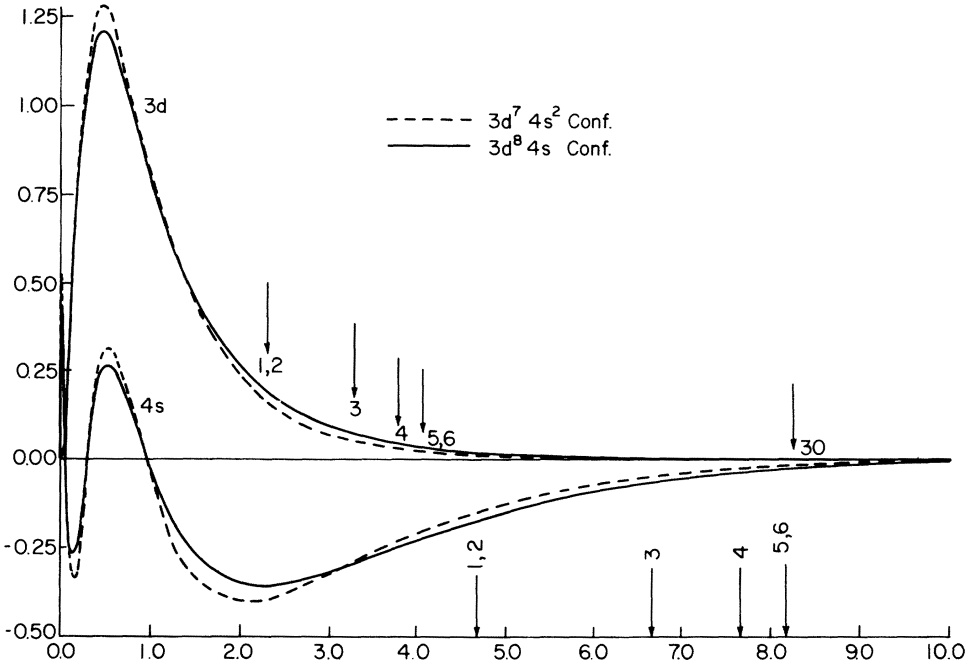

FIG. 2. Wave functions for $3d$ and $4s$ atomic states in configuration $3d^8 4s$. Arrows on the r axis give the positions of the neighboring atoms and the arrows on the curve give the half of the distances to the neighboring atoms.

and the freelike electrons have nearly equal population, it is more appropriate to use $3d^{5\uparrow}3d^{3\downarrow}4s^{1/2\uparrow}4s^{1/2\downarrow}(^3F)$ configuration, which is closest to the population distribution in the metal. The radial functions $P_{nl}(r)$ for $1s$, $2s$, $2p$, $3s$, $3p$, $3d$, and $4s$ orbitals were obtained by self-consistent numerical solution of the restricted Hartree-Fock[24] equations, with spin-independent orbitals, for the average of the configurations $3d^{5\uparrow}3d^{3\downarrow}4s^{1\uparrow}(^4F)$ and $3d^{5\uparrow}3d^{3\downarrow}4s^{1\downarrow}(^2F)$, which is equivalent to using the ^3F configuration. For the sake of comparison, the $3d$ and $4s$ orbitals from this calculation are plotted against r in Fig. 2 along with the orbitals corresponding to the free atom configuration $3d^7 4s^2(^4F)$, taken from tables of analytic wave functions obtained by Clementi.[26] We see that the $3d$ and $4s$ functions are more spread out for the configuration corresponding to the metal than for the free atom case. This diffuseness assists[30] in the binding in the metal through a lowering of kinetic energy and increased interaction between atoms.

For our work in the metal, we shall make use of this newly determined $3d$ function. However, in calculating the Coulomb and exchange potential matrix elements, the diffuse nature of these $3d$ orbitals leads to substantial overlap between orbitals on adjacent atoms and can require the calculation of a large number of two-, three-, and four center integrals. The calculation of these multicenter integrals involving explicit overlap between two and more atoms is rather time consuming.[1] We shall avoid calculating these integrals explicitly by breaking up the $3d$ function into two parts, as in Fig. 3, namely a tightly packed function with no overlap between atoms and a diffuse tail function. The tail function will be expanded in a series of plane waves. Thus, the right binding function of the form (2.12) constructed out of atomic $3d$ orbitals now becomes a linear combination of a tight binding function constructed from the truncated $3d$ function and plane-wave wave functions.

We shall use the notation $\Pi_{nl}(r)$ for the nonoverlapping radial functions, including the cores which do not overlap anyway and the truncated $3d$ orbitals. The tight-binding functions built out of these $\Pi_{nl}(r)$ shall be referred to as $\phi_{nlm\rho,\vec{k}}$. As far as the core and $3d_m$ tight-binding functions are concerned, the basis set to be used in our variational calculations for band functions will then be composed of the 18 $\phi_{nlm\rho,\vec{k}}$ functions constructed from the $1s$, $2s$, $2p_m$, $3s$, and $3p_m$ core functions and the 10 $\phi_{3dm\rho,\vec{k}}$ functions. This set will be complemented by 23 plane-wave wave functions $PW_{\vec{k}+\vec{K}}$ corresponding to the 23 shortest values of $\vec{K}$, the same set that is used for the expansion of the tail part of the $3d$ atomic function into plane waves.

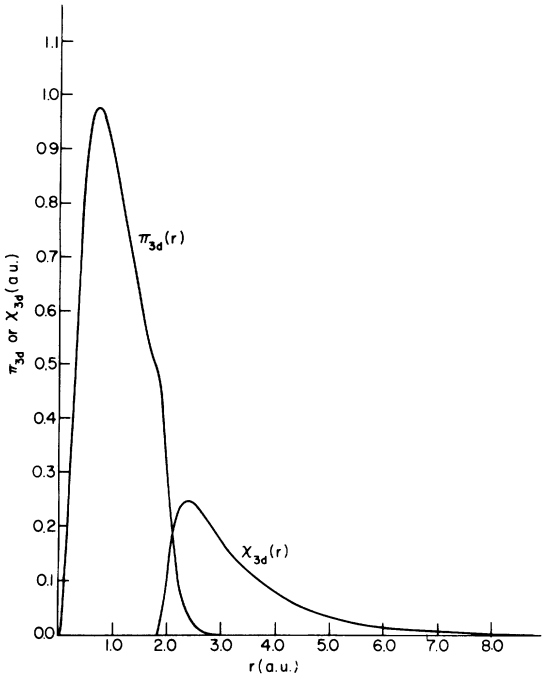

FIG. 3. Truncated $3d$ radial function, $\Pi_{3d}(r)$ and the tail part $\chi_{3d}(r)$ of the $3d$ radial function. Function $\Pi_{3d}(r)$ is normalized to unity.

B. Evaluation of overlap and Hamiltonian matrices

We shall next discuss the evaluation of the overlap (S) and Hamiltonian (H) matrices. Considering first the S matrix, the plane-wave basis states $\mathrm{PW}_{\vec{k}+\vec{K}}$ are obviously orthonormal. Also, because of negligible interatomic overlaps, the tight-binding functions $\phi_{nlmp,\vec{k}}$ can be taken as orthonormal as well. Thus,

$$\langle \phi_{nlmp,\vec{k}} | 1 | \phi_{n'm'p',\vec{k}'} \rangle = \delta_{\vec{k},\vec{k}'}\delta_{n,n'}\delta_{l,l'}\delta_{m,m'}\delta_{p,p'} \tag{2.15}$$

and

$$\langle \phi^{\mathrm{PW}}_{\vec{k}+\vec{K}} | 1 | \phi^{\mathrm{PW}}_{\vec{k}'+\vec{K}'} \rangle = \delta_{\vec{k},\vec{k}'}\delta_{\vec{K},\vec{K}'} . \tag{2.16}$$

However, the $\phi^{\mathrm{PW}}_{\vec{k}+\vec{K}}$ and $\phi_{nlmp,\vec{k}}$ functions are not orthogonal to each other, the overlap integrals between them being given by:

$$\langle \phi_{nlmp,\vec{k}} | 1 | \phi^{\mathrm{PW}}_{\vec{k}+\vec{K}} \rangle = \frac{4\pi}{\sqrt{\Omega}} (i)^l \tfrac{1}{2} (e^{-i\vec{K}\cdot\vec{\rho}/2} + p e^{+i\vec{K}\cdot\vec{\rho}/2}) \times Y^*_{lm}(\hat{e}_{\vec{k}+\vec{K}}) \int j_l(|\vec{k}+\vec{K}|r) r \Pi_{nl}(r)\, dr , \tag{2.17}$$

where $\hat{e}_{\vec{k}+\vec{K}}$ is a unit vector along $\vec{k}+\vec{K}$. For the H matrix, we have to evaluate matrix elements of the kinetic energy, nuclear potential, and Coulomb and exchange interaction energies among the electrons. The kinetic energy matrix elements are easy to evaluate and are given in Rydberg units by:

$$\langle \phi_{nlmp,\vec{k}} | -\nabla^2 | \phi_{n'l'm'p',\vec{k}} \rangle = \delta_{pp'}\delta_{ll'}\delta_{mm'} \left(\int \Pi_{nl}(r)\Pi_{n'l'}(r) \frac{l(l+1)}{r^2}\, dr - \int \Pi_{nl}(r) \frac{d^2}{dr^2} \Pi_{n'l'}(r)\, dr \right), \tag{2.18}$$

$$\langle \phi^{\mathrm{PW}}_{\vec{k}+\vec{K}} | -\nabla^2 | \phi^{\mathrm{PW}}_{\vec{k}+\vec{K}'} \rangle = |\vec{k}+\vec{K}|^2 \delta_{\vec{K},\vec{K}'}, \tag{2.19}$$

and

$$\langle \phi_{nlmp,\vec{k}} | -\nabla^2 | \phi^{\mathrm{PW}}_{\vec{k}+\vec{K}} \rangle = |\vec{k}+\vec{K}|^2 \langle \phi_{nlmp,\vec{k}} | 1 | \phi^{\mathrm{PW}}_{\vec{k}+\vec{K}} \rangle . \tag{2.20}$$

It is to be noted that both in the case of matrix elements of unity and of $-\nabla^2$, no two-center integrals occur with our choice of basis states. The potential due to the nuclear charge ζ of 27 protons at each lattice site, for any electron, which is attractive in nature, is given by:

$$Z(\vec{r}) = -\zeta \sum_j \left(\frac{2}{|\vec{r} - \vec{R}_j + \frac{1}{2}\vec{\rho}|} + \frac{2}{|\vec{r} - \vec{R}_j - \frac{1}{2}\vec{\rho}|} \right), \tag{2.21}$$

with the following matrix elements between the tight-binding basis functions:

$$\langle \phi_{nlmp,\vec{k}} | Z(\vec{r}) | \phi_{n'l'm'p',\vec{k}} \rangle = -\zeta \delta_{ll'}\delta_{mm'}\delta_{pp'} \int \frac{2}{r} \Pi_{nl}(r)\Pi_{n'l}(r)\, dr - \zeta \sum_{l''} \frac{2\times 4\pi}{2l''+1} \langle lm | l'm', l''m-m' \rangle \int r^{l''} \Pi_{nl}(r)\, \Pi_{n'l}(r)\, dr \times \sum_j \left[\frac{1}{2}(1+pp') \frac{1}{|\vec{R}_j|^{l''+1}} \text{ , or } \frac{1}{2} \frac{[pp' + (-1)^{l+l'}]}{|\vec{R}_j + \vec{1}|^{l''+1}} \right] \times (-1)^{l''} Y^*_{l'', m-m'}(\hat{e}_{\vec{R}_j} \text{ , or } \hat{e}_{\vec{R}_j + \vec{\rho}}), \tag{2.22}$$

where

$$\langle lm\,|\,l'm',\,l''m-m'\rangle$$

$$=\int Y^{*}_{lm}(\theta,\phi)\,Y_{l'm'}(\theta,\phi)\,Y_{l'',m-m'}(\theta,\phi)\sin\theta\,d\theta\,d\phi\,. \tag{2.23}$$

The right-hand side of Eq. (2.22) is independent of $\vec{k}$. The summation on l'' in Eq. (2.22) is limited by angular momentum and parity conservation rules. The summation on j is over all lattice sites (this includes both the atoms in the unit cell and all the unit cells). In all the matrix elements, values of j corresponding to 38 neighbor atoms plus the central atom ($j=0$) at which the atomic orbital is located, are included. The contribution from the distant atoms is very nearly cancelled (to about 0.0015 Ry) by a similar contribution from the Coulomb potential due to the electrons, with opposite sign. The choice of the term in the large square brackets in Eq. (2.22) is decided by the nature of the interatomic vector $\vec{R}_{j0}$. For $\vec{R}_{j0}=\vec{R}_n$, the first term is to be taken, while for $\vec{R}_{j0}=\vec{R}_n+\vec{\rho}$, the second is the appropriate term. A corresponding choice is made for the argument of the spherical harmonic involving the lattice coordinates. This kind of dual set of terms will appear in later matrix elements also and a similar procedure will be adopted there. The hybrid matrix elements

$$\langle\phi_{nlmp,\vec{k}}\,|Z(\vec{r})\,|\,\phi^{\mathrm{PW}}_{\vec{k}+\vec{K}}\rangle$$

can be similarly obtained by expanding the PW in Bessel functions and spherical harmonics.

$$e^{i(\vec{k}+\vec{K})\cdot\vec{r}}=\sum_{lm}4\pi(i)^l\,Y^{*}_{lm}(\hat{e}_{\vec{k}+\vec{K}})\times Y_{lm}(\hat{r})\,j_l(|\vec{k}+\vec{K}|r)\,. \tag{2.24}$$

The matrix elements of the nuclear Coulomb potential between two plane waves is the next one to be considered and the diagonal and off-diagonal elements are evaluated separately. For the off-diagonal case one obtains:

$$\langle\phi^{\mathrm{PW}}_{\vec{k}+\vec{K}}\,|Z(\vec{r})\,|\,\phi^{\mathrm{PW}}_{\vec{k}+\vec{K}}\rangle$$

$$=-\frac{2\times4\pi\zeta}{\Omega\,|\vec{K}-\vec{K}'|^2}\cos[(\vec{K}-\vec{K}')\cdot\tfrac{1}{2}\vec{\rho}]\ \text{ for }\vec{K}\neq\vec{K}'\,, \tag{2.25}$$

while for the diagonal case one gets the divergent result

$$\langle\phi^{\mathrm{PW}}_{\vec{k}+\vec{K}}\,|Z(\vec{r})\,|\,\phi^{\mathrm{PW}}_{\vec{k}+\vec{K}}\rangle=-\frac{\zeta}{\Omega}\int\frac{2}{r}\,d^3r\,. \tag{2.26}$$

The divergence is owing to the fact that the integral on the right-hand side extends over the entire volume of the crystal. This divergence is not of any concern,[1] since it arises because of the long-range character of the nuclear Coulomb potential and is completely cancelled by a similar divergent term coming from the electronic Coulomb potential, as discussed subsequently in this section.

We turn next to the matrix elements for the electron-electron interactions. These involve the potential due to the electrons and for the latter, we need a knowledge of the electron distribution. However, to get the electronic distribution we need, in turn, to know the potential, and this is a typical self-consistency problem, to be discussed in Sec. IV. To start the calculation, one has to make an initial choice of the populations in majority- and minority-spin $3d$ and freelike bands. Thus, from the earlier band calculations of Wakoh and Yamashita[2] for the paramagnetic phase with a rigid band shift to give ferromagnetism, one finds that the bands that look $3d$-like are completely filled for the majority spin, while the corresponding minority bands are only partially full. Also, as a first approximation, one can assume that the total magnetic moment of $1.56\mu_B$ per atom is due entirely to $3d$-like electrons. Thus, of the total of nine valence electrons, one makes the initial assignment of five electrons to majority-spin $3d$ states, 3.44 electrons to minority-spin $3d$ states, and 0.28 each in the majority- and minority-spin freelike bands. In addition to this, of course, there are 18 core electrons in states $\phi_{nlmp,\vec{k}}$ with nine for each spin.

Using this choice of populations, one can construct the initial density matrix. The general form of the density matrix elements, at any stage of iteration, can be obtained using the eigenfunctions corresponding to band t, reduced vector $\vec{k}$, and spin σ defined in Eq. (2.14), and have the forms:

$$P_{nlmp,n'l'm'p',\vec{k}t\sigma}=\tfrac{1}{2}C^{*}_{\vec{k}t\sigma,nlmp}C_{\vec{k}t\sigma,n'l'm'p'}\,,$$
$$P_{\vec{K},\vec{K}',\vec{k}t\sigma}=\tfrac{1}{2}C^{*}_{\vec{k}t\sigma,\vec{K}}C_{\vec{k}t\sigma,\vec{K}'}\,, \tag{2.27}$$

for the matrix elements purely in tight-binding space and plane-wave space, respectively, and

$$P_{nlmp,\vec{K},\vec{k}t\sigma}=\tfrac{1}{2}C^{*}_{\vec{k}t\sigma,nlmp}C_{\vec{k}t\sigma,\vec{K}}, \tag{2.28}$$

for the hybrid elements involving the two spaces. The factor of one-half is included to take account of the fact that there are two atoms per unit cell.

Lastly, before proceeding to the calculation of the Coulomb and exchange matrix elements, we should remark that we need a summation over occupied $\vec{k}$ states. For this purpose, we transform the density matrix for a value of $\vec{k}$ within the $\frac{1}{24}$th Brillouin zone (BZ), shown in Fig. 4, to the other $\vec{k}$ vectors belonging to the star of $\vec{k}$ and contained in the 23 other segments of the Brillouin zone. This transformation can be accomplished by using the trans-

formation properties of the coefficients $C_{\vec{k}t\sigma,nlmp}$ and $C_{\vec{k}t\sigma,\vec{K}}$. Thus, we consider for example summations over all $\vec{k}$ for the density matrix elements between purely tight-binding states and purely plane-wave states as given by:

$$P_{nlmp,n'l'm'p',\sigma} = \sum_{\substack{\vec{k}\,t \\ \text{occupied states}}} \frac{1}{N} P_{nlmp,n'l'm'p',\vec{k}t\sigma}$$

and (2.29)

$$P_{\vec{K},\vec{K}',\sigma} = \sum_{\substack{\vec{k}\,t \\ \text{occupied states}}} \frac{1}{N} P_{\vec{K},\vec{K}',\vec{k}t\sigma},$$

which occur in the Coulomb integrals. Using the symmetry operations of the hcp lattice, one can show[30] that Eqs. (2.29) take the form

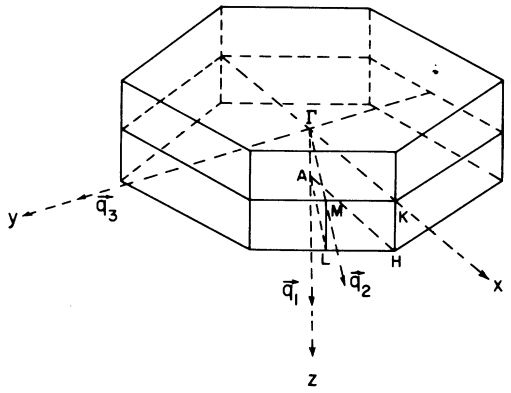

FIG. 4. Reciprocal lattice, first Brillouin zone, and the irreducible part $\Gamma MKHAL\Gamma$ of the Brillouin zone.

$$P_{nlmp,n'l'm'p',\sigma} = \sum_{t}\sum_{\substack{\vec{k} \\ \text{occupied states in } \frac{1}{24}\text{th of BZ}}} \frac{1}{N}\{1+2\cos[(m-m')\tfrac{2}{3}\pi]\}[1+(-1)^{l+l'+m+m'}][1+(-1)^{l+l'}pp'] \times (P_{nlmp,n'l'm'p',\vec{k}t\sigma} + e^{i(m-m')\pi/3} P^{*}_{nlmp,n'l'm'p',\vec{k}t\sigma}) \tag{2.30}$$

and

$$P_{\vec{K},\vec{K}',\sigma} = e^{i(\vec{K}'-\vec{K})\cdot\vec{\rho}/2} \sum_{t}\sum_{\substack{\vec{k} \\ \text{occupied states in } \frac{1}{24}\text{th of BZ}}} \sum_{O_j} e^{-iO_j(\vec{K}'-\vec{K})\cdot\vec{\rho}/2}(P_{O_j\vec{K},O_j\vec{K}',\vec{k}t\sigma} + P_{-O_j\vec{K},-O_j\vec{K}';\vec{k}'t\sigma}), \tag{2.31}$$

where O_j is the jth group operation, $j=1-12$ and excludes the inversion operation.

In obtaining the Coulomb and exchange matrix elements, given by J_{mn} and K_{mn} in Eq. (2.6), in forms convenient for calculation, it is useful to define one- and two-electron density functions, namely, $\rho(\vec{r})$ and $\rho^{\sigma}(\vec{r}_1,\vec{r}_2)$ including summations of terms involving density matrices and basis set wave functions over the occupied core, $3d$, and conduction-band states.

$$\rho(\vec{r}_1) = 2\sum_{\substack{nlmp \\ n'l'm'p'}}\sum_{\vec{k}\sigma}\sum_{t} P_{nlmp,n'l'm'p',\vec{k}t\sigma}\phi^{*}_{nlmp,\vec{k}}(\vec{r}_1)\,\phi_{n'l'm'p',\vec{k}}(\vec{r}_1) + 2\sum_{\vec{K},\vec{K}'}\sum_{\vec{k}\sigma}\sum_{t} P_{\vec{K},\vec{K}',\vec{k}t\sigma}\phi^{PW*}_{\vec{k}+\vec{K}}(\vec{r}_1)\,\phi^{PW}_{\vec{k}+\vec{K}}(\vec{r}_1)$$
$$+ 2\sum_{nlmp}\sum_{\vec{K},\vec{k}\sigma}\sum_{t} P_{nlmp,\vec{K},\vec{k}t\sigma}\phi^{*}_{nlmp,\vec{k}}(\vec{r}_1)\,\phi^{PW}_{\vec{k}+\vec{K}}(\vec{r}_1) + 2\sum_{nlmp}\sum_{\vec{K},\vec{k}\sigma}\sum_{t} P^{*}_{nlmp,\vec{K},\vec{k}t\sigma}\phi^{PW*}_{\vec{k}+\vec{K}}(\vec{r}_1)\,\phi_{nlmp,\vec{k}}(\vec{r}_1) \tag{2.32}$$

and

$$\rho^{\sigma}(\vec{r}_1,\vec{r}_2) = 2\sum_{\substack{nlmp \\ n'l'm'p'}}\sum_{\vec{k}}\sum_{t} P_{nlmp,n'l'm'p',\vec{k}t\sigma}\phi^{*}_{nlmp,\vec{k}}(\vec{r}_1)\,\phi_{n'l'm'p',\vec{k}}(\vec{r}_2) + 2\sum_{\vec{K},\vec{K}'}\sum_{\vec{k}}\sum_{t} P_{\vec{K},\vec{K}',\vec{k}t\sigma}\phi^{PW*}_{\vec{k}+\vec{K}}(\vec{r}_1)\,\phi^{PW}_{\vec{k}+\vec{K}}(\vec{r}_2)$$
$$+ 2\sum_{nlmp,\vec{K}}\sum_{\vec{k}}\sum_{t} P_{nlmp,\vec{K},\vec{k}t\sigma}\phi^{*}_{nlmp,\vec{k}}(\vec{r}_1)\,\phi^{PW}_{\vec{k}+\vec{K}}(\vec{r}_2) + 2\sum_{nlmp,\vec{K}}\sum_{\vec{k}}\sum_{t} P^{*}_{nlmp,\vec{K},\vec{k}t\sigma}\phi^{PW*}_{\vec{k}+\vec{K}}(\vec{r}_1)\,\phi_{nlmp,\vec{k}}(\vec{r}_2). \tag{2.33}$$

There are three families of Coulomb potential matrix elements, namely,

$$\langle\vec{k}+\vec{K}\,|\,V_{\text{Coul}}\,|\,\vec{k}+\vec{K}'\rangle = \langle\phi^{PW}_{\vec{k}+\vec{K}}(\vec{r}_1)\,|\int\rho(\vec{r}_2)\frac{e^2}{r_{12}}d^3r_2\,|\,\phi^{PW}_{\vec{k}+\vec{K}}(\vec{r}_1)\rangle, \tag{2.34}$$

$$\langle nlmp,\vec{k}\,|\,V_{\text{Coul}}\,|\,n'l'm'p',\vec{k}\rangle = \langle\phi_{nlmp,\vec{k}}(\vec{r}_1)\,|\int\rho(\vec{r}_2)\frac{e^2}{r_{12}}d^3r_2\,|\,\phi_{n'l'm'p',\vec{k}}(\vec{r}_1)\rangle, \tag{2.35}$$

$$\langle nlmp,\vec{k}\,|\,V_{\text{Coul}}\,|\,\vec{k}+\vec{K}\rangle = \langle\phi_{nlmp,\vec{k}}(\vec{r}_1)\,|\int\rho(\vec{r}_2)\frac{e^2}{r_{12}}d^3r_2\,|\,\phi^{PW}_{\vec{k}+\vec{K}}(\vec{r}_1)\rangle. \tag{2.36}$$

The exchange interaction matrix elements needed for the Hamiltonian matrix are listed below, the V^{σ}_{ex} operator on the left-hand side being nonlocal[1] in nature.

$$\langle \vec{k}+\vec{K}|V^{\sigma}_{ex}|\vec{k}+\vec{K}\rangle = \int d^3r_1\, d^3r_2\, \phi^{PW*}_{\vec{k}+\vec{K}}(\vec{r}_2)\rho^{\sigma}(\vec{r}_1,\vec{r}_2)\frac{e^2}{r_{12}}\phi^{PW}_{\vec{k}+\vec{K}'}(\vec{r}_1)\,, \tag{2.37}$$

$$\langle nlmp,\vec{k}|V^{\sigma}_{ex}|n'l'm'p',\vec{k}\rangle = \int d^3r_1\, d^3r_2\phi^{*}_{nlmp,\vec{k}}(\vec{r}_2)\,\rho^{\sigma}(\vec{r}_1,\vec{r}_2)\frac{e^2}{r_{12}}\phi_{n'l'm'p',\vec{k}}(\vec{r}_1)\,, \tag{2.38}$$

and

$$\langle nlmp,\vec{k}|V^{\sigma}_{ex}|\vec{k}+\vec{K}\rangle = \int d^3r_1\, d^3r_2\,\phi^{*}_{nlmp,\vec{k}}(\vec{r}_2)\,\rho^{\sigma}(\vec{r}_1,\vec{r}_2)\frac{e^2}{r_{12}}\phi^{PW}_{\vec{k}+\vec{K}}(\vec{r}_1)\,. \tag{2.39}$$

On substituting the expression for $\rho(\vec{r})$ from Eq. (2.32) into Eqs. (2.34)–(2.36) and the expression for ρ^{σ} from Eq. (2.33) into Eqs. (2.37)–(2.39), we get more explicit expressions for each of the interaction matrix elements. We will not present these elaborate equations[30] here, but instead include the important steps in their derivation in the appendix.

III. INCORPORATION OF CORRELATION EFFECTS IN BAND CALCULATION

In this section, the incorporation of the electron-electron correlation effects into the electronic band structure will be discussed. The procedure followed involves a combination of different methods applicable for the variety of pair-correlation interactions, involving electrons in core states, d-bands, and conduction bands, that we have to be concerned with. For correlation effects involving core electrons interacting with other core electrons, d-band electrons, or freelike electrons and d-electrons interacting with freelike band electrons, we shall make use of atomic many-body perturbation theory.[19,20,34] For interactions between d-band electrons, we have used a bandwidth-dependent Hubbard correlation treatment[21] applied earlier to iron.[1] For correlation effects involving only freelike electrons, the results of a recently developed self-consistent many-body procedure by the authors[22] will be utilized. This treatment of correlation effects among freelike electrons is different from that utilized for iron. Also the correlation effects between core and $3d$ electrons (except for intraband effects) were not considered for iron but are included in the present calculation. The description of these types of correlation will therefore be described here. For the intraband correlation, we shall follow the procedure developed in the earlier work on iron[1] for adaptation of the Hubbard treatment for narrow bands. Only a few remarks will be added in this case for the sake of completeness.

A. Correlation corrections freelike electrons

To find the correlation corrections to the energy of freelike electrons, we have to consider pair excitations involving the electron in question paired with each of the other electrons in occupied states. The freelike electron wave function looks very much like the atomic $4s$ electron wave function near the atom, while in the region in between two atoms it looks like a plane wave. So to a good approximation we can consider the core and $3d$ electron correlations with the freelike electrons to be represented by correlations of core and $3d$ electrons with the $4s$ electron in a free atom in the configuration $3d^{8.5}4s^{0.5}$ which corresponds closest to the metal. The numerical results for this type of correlation energy can be taken from many-body diagrams for neutral manganese and iron atoms[34] with population adjusted for the cobalt configuration considered above and appear in the last row of Table I. Between the two, man-

TABLE I. Atomiclike correlation energy corrections for core one-electron states in cobalt metal. Unit of energy is one rydberg.

State	Spin up[a]	Spin down
$1s$	−0.043 37	−0.052 59
$2s$	−0.139 70	−0.148 92
$2p$	−0.220 69	−0.232 71
$3s$	−0.139 33	−0.148 55
$3p$	−0.226 69	−0.238 71
$3d$	−0.266 72	−0.314 33
$4s$[b]	−0.100 57	−0.105 68
$3d$[c] (Hubbard)	0.000 00	−0.398 20

[a] Spin up refers to majority-spin directions and spin down to minority. Populations in different states used for the metal are $3d^{5\uparrow}$, $3d^{3.5\downarrow}$, $4s^{0.25\uparrow}$, $4s^{0.25\downarrow}$ with the core states completely full.

[b] The $4s$ state correlation energy listed does not include $4s$-$4s$ correlation energy, which is −0.100 32 Ry. Instead we add free-electron correlation energies to the diagonal matrix elements as explained in the text.

[c] This represents the Hubbard correlation energy.

ganese and iron atoms, the latter was used in our calculation because its configuration is somewhat closer to that of the cobalt configuration of interest to us. For the correlation corrections due to interaction between freelike electrons, the values obtained earlier[22] for a uniform electron gas are used by choosing the appropriate r_s for the electron density in the metal. This density was determined by using the number of electrons per atom as equal to the number of freelike electrons plus the contribution from the plane-wave components of the $3d$ band electrons to take care of their delocalization. Thus,

$$(N_{\text{free}})_{\text{eff}} = 9.0 - \sum_{m\rho\sigma} P_{3dm\rho,3dm\rho,\sigma}. \tag{3.1}$$

This number gives an effective r_s between 2 and 3 depending on the density matrix elements in Eq. (3.1) at the appropriate iteration cycle. The correlation energy corrections for $r_s = 2$ and 3 for different values of k are given in Table II and for intermediate values of r_s one could interpolate between these two tables. Since we have, for our $3d$-like electrons in the crystal, significant hybridization of the $3d$ basis states with plane-wave states, this hybridization causes the $3d$ electrons to become itinerant and therefore in the present procedure, the conduction-electron correlation approximately includes the correlation occurring between itinerant parts of the $3d$ states as well as between the latter and the freelike states.

The sum of the atomic-type correlation energies and the PW type correlation energy considered above gives the net correlation energy for a PW state. In this case, as well as in the others discussed in this section, we introduce this correction in the diagonal elements of the Hamiltonian matrix, and this leads to three advantages over doing a simple addition of the correlation correction to the conduction-state eigenvalue. The first advantage is that, because the actual eigenstate has different PW's mixed together and the correlation for each of them is different, this is a simple way to incorporate its effect. The other benefit of this procedure is that the hybridization of various basis states gets properly readjusted because of the changed energy values corresponding to these states, which in perturbation theory means correcting the energy denominator for self-energy-like effects. Also, since overlap of $3d$-like electrons from neighboring atoms is simulated through their mixing with plane waves, the correlation energy between the plane-wave components of the $3d$ states simulates the effect of the interatomic $3d$ correlations.

TABLE II. Correlation energy corrections (ε_k^c) for one-electron energies for a uniform electron gas. k is in units of $2\pi/a_0$ and ε_k^c is in units of 2 Ry.

$r_s = 2$		$r_s = 3$	
k	ε_k^c	k	ε_k^c
0.00	−0.0196	0.00	−0.0166
0.0709	−0.0361	0.0427	−0.0273
0.1089	−0.0614	0.0675	−0.0432
0.1292	−0.1010	0.0819	−0.0680
0.1401	−0.1436	0.0902	−0.0956
0.1460	−0.1657	0.0951	−0.1092
0.1527 ($=k_F$)	−0.1882	0.1018 ($=k_F$)	−0.1410
0.1560	−0.1960	0.1051	−0.1478
0.1630	−0.2050	0.1114	−0.1631
0.1730	−0.2150	0.1197	−0.1698
0.2060	−0.2365	0.1351	−0.1783
0.2680	−0.2575	0.1500	−0.1829
0.3840	−0.2633	0.1800	−0.1894

B. Correlation corrections for atomiclike electrons

The core-electron states in the metal are not much different from those in the neutral atom and so we can use the results of the atomic calculation. As mentioned earlier, results are available for neutral iron and manganese atoms[34,35] and we would like again to extend those for iron, which is closer to cobalt than is manganese, to apply to the particular configuration of cobalt that we are interested in. This requires some simplifying assumptions. First we restrict ourselves to pair excitation results only. The next assumption is that the correlation energy between pairs of electrons in a subshell of a given spin is independent of the m_l and $m_{l'}$ of the electronic states, which appears to be a reasonable approximation from pair correlation studies in iron[34] and manganese atoms[35] and ferric ion.[36] The last assumption is that this pair correlation energy for a given pair does not change appreciably in going from iron to cobalt.[34]

To illustrate the procedure we have used for obtaining the core correlation energies $\varepsilon_{nl\sigma}^c$ that enter the diagonal components of the submatrix of the Hamiltonian over the core and truncated $3d$-basis sets, we shall consider a specific example, namely, for an electron in a $3p$ state. In this case, one has to combine the correlation energies of an electron in one of these $3p$ states with (a) the electrons in all the other core states, (b) the electrons in the five other $3p$ states, and finally (c) electrons in the $3d$ and freelike states. For purposes of studying their correlation with core electrons, the freelike electrons can be regarded as $4s$ electrons. The process of obtaining $\varepsilon_{3p\sigma}^c$ then consists essentially of two steps. The first is to obtain the pair correlation energies for individual pairs

from correlation energies between shells in the iron atom. The second is to sum these pair correlation energies over all the pairs interacting with a single $3p$ electron in the cobalt metal configuration. Proceeding in this manner, one gets Eq. (3.2) for $\varepsilon^{c\uparrow}_{3p}$ for a $3p$ electron with spin parallel to the majority-spin direction.

$$\varepsilon^{c\uparrow}_{3p} = 10\,\varepsilon_{ij} + 2\varepsilon^{\mathrm{dir}}_{3p,3s} + \varepsilon^{\mathrm{ex}}_{3p,3s} + 5\varepsilon^{\mathrm{dir}}_{3p,3p} + 2\varepsilon^{\mathrm{ex}}_{3p,3p} + (N^{\uparrow}_{3d} + N^{\downarrow}_{3d})\varepsilon^{\mathrm{dir}}_{3p,3d} + N^{\uparrow}_{3d}\varepsilon^{\mathrm{ex}}_{3p,3d} + (N^{\uparrow}_{\mathrm{free}} + N^{\downarrow}_{\mathrm{free}})\varepsilon^{\mathrm{dir}}_{3p,4s} + N^{\uparrow}_{\mathrm{free}}\varepsilon^{\mathrm{ex}}_{3p,4s}\,. \tag{3.2}$$

In this equation, $N^{\uparrow}_{\mathrm{free}}$, $N^{\downarrow}_{\mathrm{free}}$, $N^{\uparrow}_{3d}$, and $N^{\downarrow}_{3d}$ correspond to the numbers of freelike and $3d$-like electrons in the metal with spins in majority and minority directions. These numbers change at each iteration and are determined initially by the $3d^{8.5}4s^{0.5}$ configuration that was stated earlier. At any intermediate cycle of iteration, we can approximately find the number of freelike and $3d$-like electrons by examining the coefficients in the band electron eigenvectors in Eq. (2.14). If in an eigenvector, the sum of the squares of the $3d$ basis function components is greater than the sum of the squares of the PW components then we can count the eigenstate as a $3d$ state and if the reverse is true, the state can be counted as a freelike state. As examples of some of the pair correlation parameters in Eq. (3.2), one can quote

$$\varepsilon^{\mathrm{dir}}_{3p,3s} = -\tfrac{1}{12}(0.163\,44)\mathrm{Ry}\,,\qquad \varepsilon^{\mathrm{ex}}_{3p,3s} = +\tfrac{1}{6}(0.067\,02)\mathrm{Ry}\,, \tag{3.3}$$

obtained from $3p$-$3s$ shell correlation energies given for iron. For the parallel spin pairs, the pair correlation energies are $\varepsilon^{\mathrm{dir}}_{3p,3s} + \varepsilon^{\mathrm{ex}}_{3p,3s}$, while for antiparallel spin pairs, the pair correlation energies are $\varepsilon^{\mathrm{dir}}_{3p,3s}$. The first term on the right-hand side in Eq. (3.2) represents the net correlation energy of a $3p$ electron arising from a sum over all pairs that the former can interact with, from within the $1s^2 2s^2 2p^6$ shell, with

$$\varepsilon_{ij} = -\tfrac{1}{160}(0.200)\mathrm{Ry} \tag{3.4}$$

for all such pairs. The number $\frac{1}{160}$ in Eq. (3.4) arises from the pairs between the 16 electrons in the $3s^2 3p^6 3d^6 4s^2$ set of shells and ten electrons in the $1s^2 2s^2 2p^6$ set of shells of iron, since only the total of the correlation energy between these two sets of shells is available.[20] For the case of $3p$ electrons with spin in the minority-spin direction (hereafter referred to as down and the majority-spin direction as up), the correlation energy $\varepsilon^{c\downarrow}_{3p}$ is obtained from Eq. (3.2) by interchanging the numbers of spin-up states, on the right side, with corresponding numbers of spin-down states.

The correlation correction to the diagonal matrix elements of the Hamiltonian for all the other localized states $1s$ through $3d$ can be obtained in the same manner as for the $3p$ state.

For the correlation parameters $\varepsilon^{c}_{4s\uparrow}$ and $\varepsilon^{c}_{4s\downarrow}$, referring to the conduction-electron states, one can obtain a similar expression as for the case of the $3p$ state. However, this expression will involve $4s$-$4s$ pair correlation energy which, in the case of metal is more appropriately represented by the pair correlation energy between plane-wave states, as discussed earlier in this section. Table I lists all the correlation parameters $\varepsilon^{c}_{nl\sigma}$ used in our calculations on the metal with two exceptions. The PW-PW pair correlation energy contribution to the conduction states which can be derived from Table II have to be added to the $\varepsilon^{c}_{4s\sigma}$ parameter to obtain the appropriate correlation energy parameter. The $3d$ correlation parameters $\varepsilon^{c}_{3d\sigma}$ do not include the intraband correlation effect which has no counterpart in the atom but is rather important for the solid. This correlation energy shall be considered next.

C. Intraband correlation for $3d$-like electrons

In the metal, pair excitations completely within the $3d$ band are allowed and they give rise to additional correlation energy if the $3d$ band is partially filled. These pair excitations cannot be ruled out by angular momentum conservation rules because the angular momentum is no longer a good quantum number, the eigenvectors now involving mixtures of various orbitals with different m_l components. Since the $3d\uparrow$ band is completely filled, we do not have any pair excitations in which both the initial and final pair states are within the $3d\uparrow$ band. For the $3d\downarrow$ band, we do have some empty states available (about 3.44 states out of 5 states per atom are filled, for the starting assumption that the spin magnetization is due to $3d$ electrons only) which lead to additional correlation. This effect will be treated here through the Hubbard[21] formulation for correlation energies in narrow bands, the adaptation of which to our present work follows the same lines as in earlier work on iron.[1] According to this formulation, the correlation correction to the diagonal matrix elements for the $3d$ tight-binding states is given by

$$\varepsilon^{c\uparrow}_{3d} = (V_c - V_{\mathrm{eff}})(\tfrac{1}{5}N^{\uparrow}_{3d} - 1)\,, \tag{3.5}$$

$$\varepsilon^{c\downarrow}_{3d} = (V_c - V_{\mathrm{eff}})(\tfrac{1}{5}N^{\downarrow}_{3d} - 1)\,, \tag{3.6}$$

where

$$V_{\mathrm{eff}} = \frac{V_c\,\frac{1}{4}\Delta}{\{(\frac{1}{2}V_c + \frac{1}{4}\Delta)^2 - \frac{1}{4}[\frac{1}{10}(N^{\downarrow}_{3d} + N^{\uparrow}_{3d})]\,V_c\Delta\}^{1/2}}\,, \tag{3.7}$$

V_c being the average Coulomb interaction integral between two different electrons in the $3d$ shell for the atomic configuration closest to the metal and Δ is the total width of the $3d$ bands. The behavior of $\epsilon^c_{3d\uparrow}$ and $\epsilon^c_{3d\downarrow}$ in the limits may be seen by noting that for $\Delta \to 0$, we get $V_{\text{eff}} \to 0$ and $\epsilon^c_{3d\uparrow}$, $\epsilon^c_{3d\downarrow}$ in Eqs. (3.5) and (3.6) approach their maximum value. If $\Delta \to \infty$, then V_{eff} becomes equal to V_c, and Eqs. (3.5) and (3.6) give zero correlation energy. The first limit for $\Delta = 0$ gives the difference in the energy per $3d$ electron between a fully localized limit for the $3d$ electron and a fully delocalized or itinerant electron, except for a small correction due to the exchange interaction between the $3d$ electrons as well. The limit of ϵ^c_{3d} in Eq. (3.6) for $\Delta = 0$ represents the maximum correlation energy possible[1,21] from intraband correlation, because in addition to the energy of a fully delocalized Bloch electron it gives essentially the energy of an atomiclike $3d$ electron which is what the band electron approximates to for a band of zero width. The lower limit of ϵ^c_{3d} in Eq. (3.6) for $\Delta = \infty$ gives zero intraband correlation energy because in this case, the energy of the $3d$ electron is that for a fully itinerant Bloch electron and the energy difference between the localized atomic $3d$ electron and the band electron has the largest possible value.

In our present work on cobalt, the majority band is completely full,[1] so that $\frac{1}{5}N_{3d\uparrow} - 1 = 0$. The minority band is not filled and is the only one for which intraband correlation effects are to be considered. The total width Δ of the minority $3d$ band (not just the width of the occupied part of the band) can be estimated from the density of states plots. The value of V_c using Π_{3d} orbitals is 1.893 Ry. To estimate V_c for the band $3d$ states we proceed as follows. The Coulomb interaction between two $3d$ electrons on one atom would be small if the $3d$ wave functions are very much spread outwards and will be large if they are closely packed. We estimate the value of V_c by calculating the fractional amount of the localized component, corresponding to Π_{3d}, per atom, in the crystal as

$$x = \sum_{mp} P^{\downarrow}_{3dmp,\,3dmp} / N^{\downarrow}_{3d} \tag{3.8}$$

and then using

$$V_c = 1.893\left[\tfrac{1}{3}(1+2x)\right]. \tag{3.9}$$

The complete correlation energy for a $3d$ down spin state is the sum of the atomiclike correlation energy, discussed in Sec. III B for the $3d$ state and the band correlation energy given in Eq. (3.6).

IV. SELF-CONSISTENCY

The importance of the requirement of self-consistency in the band calculation has already been discussed in Sec. II. The calculation is started with the assumed electron distribution described in Sec. II, namely, 5.00 $3d\uparrow$ electrons and 3.44 $3d\downarrow$ electrons and 0.28 electrons in OPW states of each spin per atom. The core states were all assumed to be occupied. The wave functions for all the atomic orbitals were obtained from a self-consistent Hartree-Fock calculation[30] for the cobalt atom in the $3d^{5\uparrow}3d^{3\downarrow}4s^{0.5\uparrow}4s^{0.5\downarrow}(^3F)$ configurations. Using these numbers and following the steps indicated in Sec. II, the density matrices $P_{nlmp,n'l'm'p',\vec{k}\sigma}$, $P_{nlmp,\vec{k},\vec{k}\sigma}$ were evaluated. Using these density matrices, the Coulomb and exchange interaction matrix elements were computed as described in Sec. II to get the Hamiltonian matrix. The H matrix was of order 51 because of 28 tight-binding functions and 23 plane-waves. The correlation corrections were added to the diagonal elements of the H matrix according to the steps in Sec. III. For the estimation of these correlation corrections, the populations in the truncated $3d$ states are needed. These populations were evaluated for the first cycle from the initial choice of density matrices at the various points in $\frac{1}{24}$th BZ, discussed in Sec. II and are given by total truncated $3d$ part with spin up,

$$\sum_{mp} P^{\uparrow}_{3dmp,\,3dmp} = 4.540 \text{ per atom},$$

and total truncated $3d$ part with spin down, (4.1)

$$\sum_{mp} P^{\downarrow}_{3dmp,\,3dmp} = 3.124 \text{ per atom}.$$

The density matrices used in Eq. (4.1) were determined by the type of eigenfunctions chosen for the electronic states. Also needed for the Hubbard correlation is the bandwidth for the down spin which was chosen to be 0.8 Ry for the first cycle. This bandwidth was chosen, very roughly, by looking at the energy levels at a few points before incorporating the Hubbard correlation correction. The other correlation energy contributions involving the core electrons and the conduction electrons were incorporated using the procedures outlined in Sec. III. The pair-correlation effects involving the core electrons did not change significantly on iteration. But the pair-correlation energy between the freelike electrons was dependent on the density matrix at each iteration and was obtained by adjusting the r_s at each iteration.

From the diagonalization of the H and S matrices, the eigenvalues and eigenvectors were ob-

tained at the 155 points in $\frac{1}{24}$th of the Brillouin zone. By summing the number of states below an assumed Fermi level ϵ_F, considering these points, and adjusting ϵ_F to get the total number of band electron states per atom to equal nine (18 in core and 9 in band), the total number of band electrons with majority spin was found to be 5.313 per atom and the number of electrons with minority spin was 3.688 per atom, giving a spin magnetization of $1.625\mu_B$ per atom. The experimental value of the magnetization[2,12] due to spin is $1.56\mu_B$ per atom. So our value of the spin magnetization, at the end of the first cycle, was quite close to the experimental value.

An additional and important dimension of self-consistency requires the eigenfunctions, which determine the Hamiltonian matrix for the next iteration, to exhibit similar self-consistency. From the occupied eigenstates, the density matrices are calculated at the same 155 points in the BZ. For a self-consistent calculation the new density matrices, at the output of any cycle should almost be the same as the ones used in the calculation of the Coulomb and exchange matrix elements at the beginning of that cycle. To test this for the first cycle, we compare some representative numbers from each set. The input and output density matrices for the first cycle are denoted by P_0 and P_1, respectively. The comparison is given in Table III and indicates that the consistency in the density matrix does need improvement. For this purpose, iterations have to be carried out in the band calculation, but rather than use the output density matrices from this cycle as the input for the next, we proceed as follows. We take the difference of P_1 and P_0 and then calculate the electronic Coulomb and exchange interaction matrices from the difference density matrices $(P_1 - P_0)$. The calculation of these Coulomb and exchange matrices is done in exactly the same way as earlier except that one does not have to incorporate the nuclear potential matrix elements with the electronic Coulomb potential matrix elements in this case since the nuclear potential matrix does not change in any cycle. One approximation that we make in the course of this iteration procedure is that we hold constant all the two-center parts of the matrix elements. The reason is that these two-center parts are only of the multipole type (since all overlap type terms, as explained earlier, have already been included through the mixing of tight-binding and plane-wave basis states) and do not change significantly with the changes in the density matrices. If we call the Hamiltonian matrices from the density matrices P_0 as H_0, and similarly the Hamiltonian matrices from the density matrices P_1 as H_1, then the Hamiltonian matrices obtained from $(P_1 - P_0)$ are actually $(H_1 - H_0)$. If we used a parameter η for characterizing a combination of P_0 and P_1 matrices to obtain the density matrices $P_0 + \eta(P_1 - P_0)$, then the corresponding Hamiltonian matrices are $H_0 + \eta(H_1 - H_0)$. The choice of η is arbitrary and is made to obtain fastest convergence. Thus, we calculate the band structure using $H_0 + \eta(H_1 - H_0)$ for various η and obtain the eigenvalues, eigenvectors, Fermi level, and then the density matrices from this second cycle, which we call $P_2(\eta)$. If $P_2(\eta)$ is close enough to $P_0 + \eta(P_1 - P_0)$, we have near self-consistency. In an investigative calculation to decide on the choice of η, the bandwidth needed for calculation of intraband (Hubbard type) correlation[1,21] for $3d$ electrons was taken as 0.50 Ry for each of up and down spins. Also, we chose $N^{\uparrow}_{3d} = 5.0$, $N^{\downarrow}_{3d} = 3.50$, $N^{\uparrow}_{\text{free}} + N^{\downarrow}_{\text{free}} = 0.50$, the other parameters needed for correlation corrections in Eqs. (3.1), (3.5), and (3.8) were determined by the choice of η. Also, for this test calculation, a fewer set of 27 points in $\frac{1}{24}$th of the BZ were used instead of the 155 points used in obtaining detailed results on the energy bands and wave functions. The test was carried out for $\eta = 0.4$, 0.45, 0.50, 0.55, 0.60 and the density matrices were evaluated in each case. Graphs of the mean square deviations, $\{P_2(\eta) - [P_0 + \eta(P_1 - P_0)]\}^2$ evaluated from these density matrices, were plotted versus η. We see from Fig. 5 that the value of η producing the least deviation is about 0.45. From these calculations, using $\eta = 0.45$ and 27 points in $\frac{1}{24}$th BZ, we find that the bandwidths for both the majority and minority bands are about 0.36 Ry for each spin. Following this analysis, we calculated the detailed band structure for all the 155 points in $\frac{1}{24}$th BZ using the value of $\eta = 0.45$ and the following values of the other parameters for the purpose of correlation corrections:

TABLE III. Comparison of the $3d$-$3d$ and PW–PW density matrices in the zeroth and the first cycles. Only the diagonal sums are considered.

Elements	P_0	P_1	Difference$(P_1 - P_0)$
$\sum_{\vec{K}} P^{\uparrow}_{\vec{K},\vec{K}}$	0.4881	1.2446	+0.7565
$\sum_{\vec{K}} P^{\downarrow}_{\vec{K},\vec{K}}$	0.4772	1.2958	+0.8486
$\sum_{m\rho} P^{\uparrow}_{3dm\rho,3dm\rho}$	4.5399	3.5600	−0.9799
$\sum_{m\rho} P^{\downarrow}_{3dm\rho,3dm\rho}$	3.1240	2.0208	−1.1032

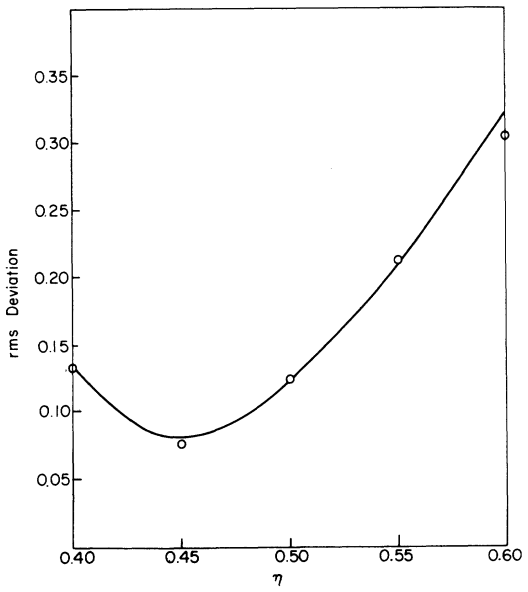

FIG. 5. Root-mean-square deviations of the density matrices vs the η parameter.

$$\Delta = 0.34 \text{ for spin down;}$$
$$N^{\uparrow}_{3d} = 5.0,\quad N^{\downarrow}_{3d} = 3.50,\quad N^{\downarrow}_{\text{free}} + N^{\downarrow}_{\text{free}} = 0.50; \tag{4.2}$$
$$\sum_{K,\sigma} P_{KK\sigma} = 1.658,\quad \sum_{m\rho} P^{\downarrow}_{3dm\rho,\,3dm\rho} = 2.628,$$
$$\sum_{m\rho} P^{\uparrow}_{3dm\rho,\,3dm\rho} = 4.009.$$

From this band structure, which we call the second cycle band structure, we have the Fermi energy equal to −0.3345 Ry and it gives a spin magnetic moment of $1.582\mu_B$ per atom in satisfactory agreement with the experimental value. Exact agreement was achieved with the experimental value of $1.560\mu_B$ for the magnetic moment by choosing slightly different $\epsilon^{\uparrow}_F$ and $\epsilon^{\downarrow}_F$, namely, $\epsilon^{\uparrow}_F = -0.340$ Ry and $\epsilon^{\downarrow}_F = -0.336$ Ry. The difference between these Fermi energies for different spin states is too small to attach much physical significance to it. However, the fact that this small difference in $\epsilon^{\uparrow}_F$ and $\epsilon^{\downarrow}_F$ is needed is an indication of the slight uncertainty in the Hubbard correlation employed due to the impreciseness of the bandwidth Δ as a parameter.

To study the self-consistency of this cycle, we compare in Table IV, again, some sample density matrix elements form $P_0 + \eta(P_1 - P_0)$ with $P_2(\eta)$. The results in this table show that in the second cycle itself, with the right choice of η, we have achieved quite good self-consistency. If further improvement is needed, one could calculate a new set of difference density matrices $P_2(\eta) - [P_0 + \eta(P_1 - P_0)]$, the potential matrix elements associated with them, and add η' times those potential matrices to $H_0 + \eta(H_1 - H_0)$, where η' could in principle be different from η and chosen in the same fashion as η was. However, we felt that the consistency obtained here was satisfactory enough for our present purposes and we did not perform any additional cycles of iteration. We shall be using the results from this second cycle to study a variety of properties of ferromagnetic cobalt.

From a density-of-states plot for spin-up and down states, (Figs. 6 and 7) we see that the width of the spin-up $3d$-like band is 0.34 Ry and the width of the $3d$-like spin-down band is also 0.34 Ry. Also we see that

$$\sum_{\vec{K}} P_{\vec{K}\vec{K},\sigma} = 1.673 \text{ and } \sum_{3dm\rho} P^{\downarrow}_{3dm\rho,\,3dm\rho} = 2.551.$$

To find the number of $3d$-like electrons and free-like electrons we take the sum of the squares of the components of an eigenvector, separately for $3d$ and PW parts. If the $3d$ part in an eigenvector is more than the PW part, we call it a $3d$-like

TABLE IV. Comparison of the input and output $3d$-$3d$ and PW–PW density matrices in the second cycle only the diagonal sums being considered.

Elements	$P_0 + 0.45(P_1 - P_0)$	$P_2(0.45)$	Difference
$\sum_{\vec{K}} P^{\uparrow}_{\vec{K},\vec{K}}$	0.8285	0.7950	−0.0335
$\sum_{\vec{K}} P^{\downarrow}_{\vec{K},\vec{K}}$	0.8291	0.8781	+0.0490
$\sum_{m\rho} P^{\uparrow}_{3dm\rho,3dm\rho}$	4.0990	4.1138	+0.0148
$\sum_{m\rho} P^{\downarrow}_{3dm\rho,3dm\rho}$	2.6280	2.5507	−0.0769

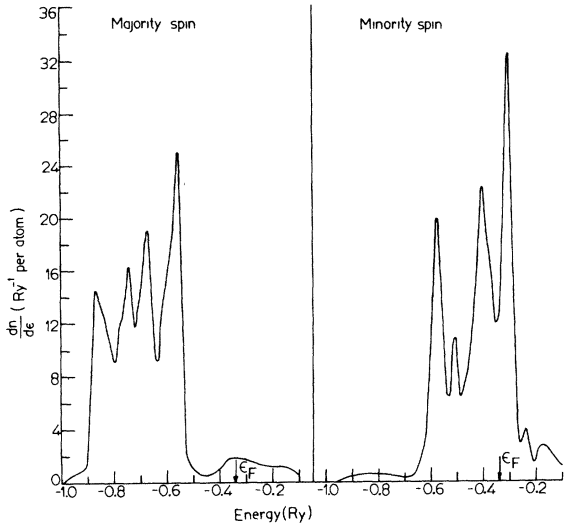

FIG. 6. Electron density of states for majority- and minority-band states. Fermi energy is −0.340 Ry.

electron state, and otherwise we label it as a freelike electron state. Proceeding this way we find

$$N^{\uparrow}_{3d}=5.033,\quad N^{\downarrow}_{3d}=3.490,$$
$$N^{\uparrow}_{\text{free}}=0.248,\quad N^{\downarrow}_{\text{free}}=0.230. \tag{4.3}$$

On comparing these with the parameters in Eq. (4.2) which were used for the evaluation of correlation corrections, we find that the calculations are quite self-consistent in this respect also.

V. BAND STRUCTURE AND ASSOCIATED PROPERTIES

A. Band structure

The shapes of the bands along the various symmetry directions from the self-consistent calculation with $\eta=0.45$ are shown in Figs. 8 and 9 for the majority and minority electrons, respectively. The convergence of the energy values was studied for some special points. Tables V and VI give the eigenvalues for point M for both the spin states. The eigenvalues are listed for the lowest ten $3d$-like levels and four freelike levels. The convergence was studied by taking 4, 8, 12, 20, and 23 plane waves in the basis set, along with the 28 tight-binding functions. We note that the overall convergence is good to nearly 0.01 Ry for all the band states. It is also clear from the tables that within the $3d$ band, for a given $\vec{k}$ point and spin direction, the uppermost levels converge faster than the lowest ones. This is because any addition of plane waves tries to lower the $3d$ levels further. For the uppermost levels, apart from this lowering the requirement of the orthogonalization of these levels to the lower ones tries to push them upwards, the two opposite moments leading to a stabilized energy. The convergence was found to be better at the Γ point than what it is at the M point. This is also expected because the higher length $(\vec{k}+\vec{k})$ vectors are somewhat more closely bunched at points closer to the boundary of the Brillouin zone than that at the Γ point and so a somewhat larger basis set is required in the former case.

The band structures in Figs. 8 and 9 for the majority- and minority-spin electrons are much more complicated than for ferromagnetic iron.[1] This is because of the hexagonal close-packed structure for cobalt, having two atoms per unit cell, while iron has a body-centered-cubic structure with only one atom per unit cell. The total overall width of the $3d$ bands is the same, about 0.34 Ry, for the majority and minority spins. On the average, the minority $3d$ bands are shifted upwards from the majority $3d$ bands by 0.29 Ry, and the splitting between the mean of the occupied parts of the majority and minority $3d$ bands is 0.23 Ry. The splitting between the freelike ma-

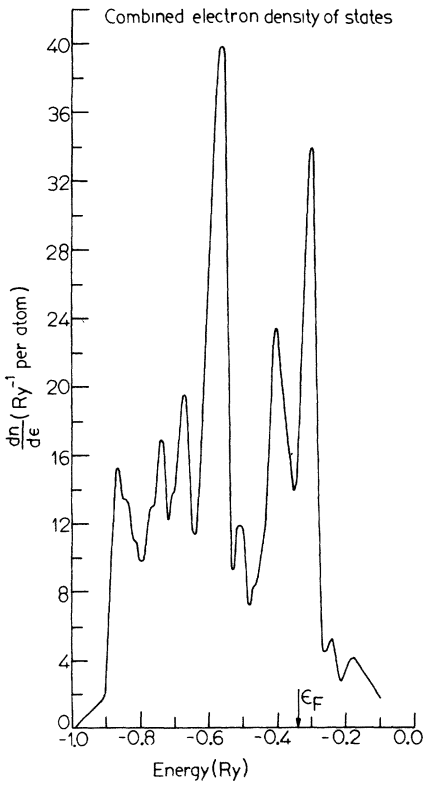

FIG. 7. Combined electron density of states for both the majority- and minority-band states. Fermi energy is −0.340 Ry.

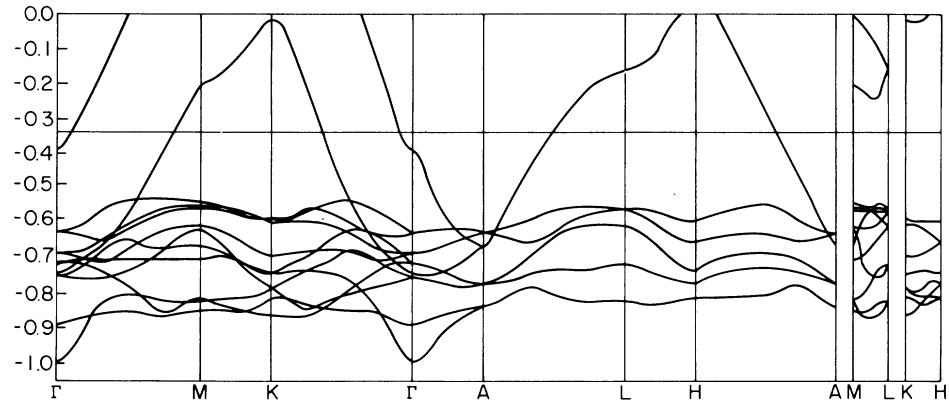

FIG. 8. Majority-spin band structure.

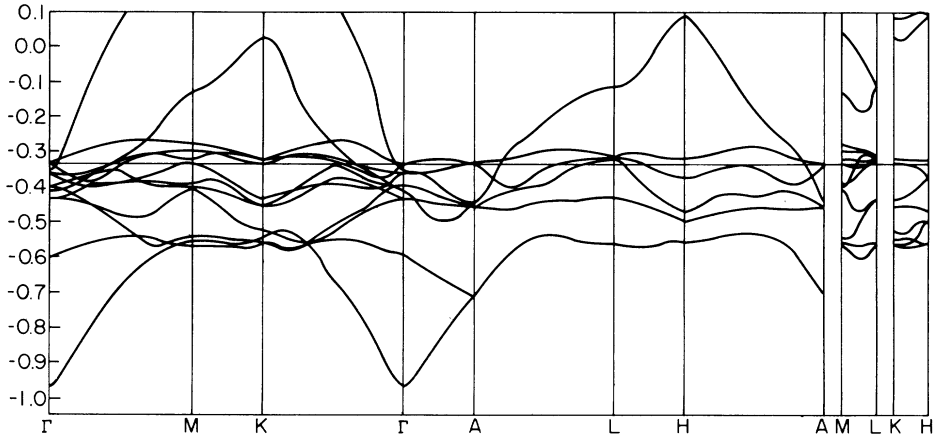

FIG. 9. Minority-spin band structure.

TABLE V. Eigenvalue convergence test (majority spin) for the size of the basis set [a] for $\vec{k}=(0.664\,77,\ 0.383\,81,\ 0.000\,00)\ a_0^{-1}$.

Band index \ Basis size	32	36	40	44	48	51
14	0.6974	0.6648	0.4841	0.4337	0.4795	0.4787
13	0.4103	0.4103	0.3720	0.3707	0.3210	0.3187
12	0.0440	0.0411	0.0240	0.0226	0.0043	−0.0047
11	−0.1739	−0.1755	−0.1843	−0.1853	−0.1970	−0.2000
10	−0.5416	−0.5416	−0.5416	−0.5419	−0.5419	−0.5422
9	−0.5480	−0.5484	−0.5490	−0.5509	−0.5512	−0.5523
8	−0.5514	−0.5525	−0.5526	−0.5535	−0.5546	−0.5571
7	−0.5583	−0.5639	−0.5730	−0.5814	−0.6048	−0.6054
6	−0.5639	−0.5668	−0.5803	−0.6036	−0.6162	−0.6169
5	−0.5803	−0.5803	−0.6084	−0.6353	−0.6633	−0.6662
4	−0.6043	−0.6056	−0.6347	−0.6471	−0.7015	−0.7015
3	−0.6739	−0.7543	−0.7568	−0.7709	−0.8083	−0.8145
2	−0.7542	−0.7570	−0.7780	−0.7825	−0.8226	−0.8226
1	−0.7543	−0.8176	−0.8417	−0.8419	−0.8466	−0.8467

[a] The number of plane waves was varied from a minimum of four to 23. In all cases 28 tight-binding functions ($1s$ to $3d$) are included. The lowest 14 eigenvalues for majority-spin states are listed for the basis size indicated on top of the column. Eigenvalues are in units of one rydberg.

TABLE VI. Eigenvalue convergence test (minority spin) for the size of the basis set[a] for $\vec{k}=(0.664\,77,\ 0.383\,81,\ 0.000\,00)\ a_0^{-1}$.

Band index \ Basis size	32	36	40	44	48	51
14	0.7296	0.675 30	0.4975	0.4966	0.4743	0.4722
13	0.4223	0.422 28	0.3989	0.3977	0.3495	0.3459
12	0.1040	0.1014	0.0825	0.0808	0.0556	0.0392
11	−0.1032	−0.1037	−0.1164	−0.1179	−0.1272	−0.1302
10	−0.2779	−0.2779	−0.2779	−0.2791	−0.2791	−0.2810
9	−0.2930	−0.2930	−0.2961	−0.2995	−0.3000	−0.3006
8	−0.2934	−0.2955	−0.2994	−0.3044	−0.3089	−0.3216
7	−0.2967	−0.2993	−0.3030	−0.3119	−0.3375	−0.3371
6	−0.2987	−0.3037	−0.3043	−0.3516	−0.3929	−0.3927
5	−0.3043	−0.3042	−0.3566	−0.3581	−0.4002	−0.4074
4	−0.3679	−0.3833	−0.3990	−0.4011	−0.4028	−0.4036
3	−0.4212	−0.4785	−0.4994	−0.5003	−0.5440	−0.5446
2	−0.4785	−0.5209	−0.5211	−0.5343	−0.5552	−0.5569
1	−0.5197	−0.5330	−0.5552	−0.5554	−0.561	−0.5706

[a] The number of plane waves was varied from a minimum of four to 23. In all cases 28 tight-binding functions ($1s$ to $3d$) are included. The lowest 14 eigenvalues for minority-spin states are listed for the basis size indicated on top of the column. Eigenvalues are in units of one rydberg.

jority and minority bands is much smaller, the minority bands being shifted by only 0.02 to 0.03 Ry upwards from the majority bands. This situation is in contrast to the equal rigid band shift of 0.126 Ry used by Wakoh and Yamashita[2] for both $3d$-like and freelike bands to obtain the majority and minority spin bands. This assumption may also be seen to be unjustified in view of the fact that the average exchange integral between two $3d$ orbitals is 0.46 Ry while that between a $3d$-like orbital and a $4s$ orbital is 0.066 Ry. Hence the exchange splittings for $3d$-like bands and freelike bands are expected to be quite different as is the case in the present calculation. This use of equal rigid band shift for $3d$-like and freelike states is perhaps the reason why paramagnetic band calculations,[2] using rigid band energy shift usually tend to predict smaller splittings between majority and minority bands than that given by ferromagnetic band calculations.[1] Further analysis shows that the splitting between various symmetry types of $3d$ bands are also different for the two spins. This comes about because of the unequal amounts of the interatomic exchange interaction and overlap effects among $3d$ eigenstates of the majority spins, in comparison to those among the $3d$ eigenstates of minority spins. In Table VII we have listed the various symmetry types and eigenvalues at the Γ point for different spins and the two different combinations involving the sum $(A+B)$ and the difference $(A-B)$ of $3d$ orbitals on the two atoms A and B

TABLE VII. Eigenvalues and the symmetry types of the states at the Γ point.[a]

Majority-spin energy	Minority-spin energy	Eigenfunction	Degeneracy
−0.3854	−0.3655	$\cos(2\pi z/c)$	1
−0.6241	−0.3322	(xz, yz) antibonding	2
−0.6852	−0.3675	(xz, yz) bonding	2
−0.7127	−0.4035	(x^2-y^2, xy) bonding	2
−0.7416	−0.4152	$(3z^2-r^2)$ bonding	1
−0.7412	−0.4378	(x^2-y^2, xy) antibonding	2
−0.8891	−0.5998	$(3z^2-r^2)$ antibonding	1
−0.9935	−0.9692	constant	1

[a] The states arising from the $3d$ atomic orbitals are indicated by their angular components. The eigenfunction with a symmetric contribution $(\psi_A+\psi_B)$ from the two basis atoms in the unit cell is referred to as bonding, and the antisymmetric combination $(\psi_A-\psi_B)$ is referred to as antibonding. Energy unit is one rydberg.

TABLE VIII. Splitting among various $3d$ states at Γ point.[a]

Symmetry type	Majority spin $A+B$	Majority spin $A-B$	Minority spin $A+B$	Minority spin $A-B$
$\mathcal{E}(xy,x^2-y^2)-\mathcal{E}(3z^2-r^2)$	0.029	0.138	0.012	0.162
$\mathcal{E}(xz,yz)-\mathcal{E}(3z^2-r^2)$	0.056	0.265	0.048	0.268
$\mathcal{E}(xz,yz)-\mathcal{E}(xy,x^2-y^2)$	0.027	0.127	0.036	0.106

[a] Energy unit is one rydberg. The symmetric combination from the two atoms in the unit cell is referred to as $A+B$, and the antisymmetric combination is referred to as $A-B$.

of the unit cell. Table VIII shows some of the $3d$-band splittings obtained from Table VII. On the basis of a rigid band model[2,4] one would have expected for example, the splitting for the $A+B$ combination for the majority-spin states to be the same as for the $A+B$ combinations for the minority-spin states (second and fourth columns of Table VIII), but there seems to be definite departure from this behavior. A similar departure is indicated by the splitting of 0.148 and of 0.185 Ry between the states of $(3z^2-r^2)_A+(3z^2-r^2)_B$ symmetry and $(3z^2-r^2)_A-(3z^2-r^2)_B$ symmetry, for the majority and minority spin cases, respectively. Thus, the actual ferromagnetic band structure departs very significantly in several respects from that obtained by a rigid band shift of paramagnetic bands.

B. Magnetization

As pointed out earlier, for the single Fermi energy (-0.3365 Ry) required to accommodate all the electrons, we get the spin magnetization as $1.582\mu_B$ per atom. This clearly shows that the present theory is able to explain very well, in a self-consistent manner, the experimental value of $1.56\mu_B$ per atom. Also, as mentioned in Sec. IV, a slight adjustment of the Fermi energies for different spins, namely, $\epsilon_F^{\uparrow}$ and $\epsilon_F^{\downarrow}$ separately as -0.340 and -0.336 Ry gives the experimental spin magnetization $1.56\mu_B$ per atom. To study the composition of this magnetization, we note that in the metal, the $3d$-like and freelike populations for spin-up and down states are given by Eq. (4.3)

This breakdown of spin population indicates that the spin magnetization $1.56\mu_B$ per atom is composed of a contribution from $3d$-like electrons of $1.543\mu_B$, and $0.017\mu_B$ from the freelike electrons. We expect the freelike electrons in the metal to be only very feebly coupled, ferromagnetically, to the $3d$-like electrons. Actually this coupling is a very delicate balance of two opposing types of interactions, as will now be discussed. From the value of the density matrices, we see that the amount of hybridization of minority $3d$ electrons (of Π_{3d} type) with plane waves is much stronger than that for the case of the majority $3d$ electrons. For an electron in a plane-wave state with spin parallel to the majority electrons, the exchange interaction arises mainly from about 4.1 localized (truncated) $3d$ electrons (Π_{3d} type) and also partially from other hybrid and itinerant parts of the majority $3d$-like electrons. For the plane-wave state with spin parallel to minority spin electrons, the exchange comes from 2.63 localized $3d$ electrons and from other hybrid and itinerant parts of the minority $3d$-like electrons. Hence, the localized parts of the $3d$ electrons tend to give stronger exchange for a spin-up plane wave. The net hybrid and itinerant parts, on the other hand, tend to give a stronger exchange for a spin-down plane wave. The latter interaction is significant since the exchange interaction of a plane wave with other plane-wave and hybrid components is much stronger than that with a localized $3d$ state. So the total exchange energy for a spin-up plane wave is not expected to be substantially different than that for a spin-down plane wave which probably explains the feeble positive polarization of the freelike electrons. At the M point, for example, the magnitude of the exchange energy for a spin-up plane wave is only 0.092 Ry more than that for spin-down plane wave. For the actual freelike electron whose wave function has mainly OPW character, the difference in exchange energies between spin-up and spin-down states is expected to be further reduced from the plane-wave value owing to the influence of the orthogonalization to core states.

Since most of the magnetic moment arises from $3d$-like electrons, we would like to discuss what our results indicate about the source of the moment on each atom and how the moments on each atom get aligned. We consider as before the $\Pi_{3d}(r)$ parts of the $3d$-like band wave functions to represent localized electrons on each site. The exchange energy of one of these localized electrons on atom A with the other localized electrons on A can be referred to as intra-atomic exchange. The rest of the exchange energy of the localized $\Pi_{3d}(r)$ electron can then be considered to arise out of interatomic exchange. To estimate the latter, one can proceed as follows: The angular average exchange energy for a $\Pi_{3d}(r)$ state (local $3d$ electron) was found from the density matrix $H_0+\eta(H_1-H_0)$ in the second cycle to be larger in magnitude for the majority spin by 0.734 Ry at the Γ point and by 0.710 Ry at the M point, as compared to the exchange energy

for a minority-spin electron. The average exchange energy difference for the two spin states from all points in the BZ, for the localized $3d$ electron, is estimated to be 0.712 Ry. The average exchange interaction of any one $\Pi_{3d}(r)$ electron with any other average $\Pi_{3d}(r)$ (meaning that the average is taken over all the five Π_{3d} states) electron is -0.461 Ry. From the values of the density matrices we find an excess of Π_{3d} type electrons of 1.471 for majority spin over the minority spin giving an excess exchange energy of 0.679 Ry more for the localized spin-up electron than spin down. This value is very close to the net exchange energy difference of 0.712 Ry given above indicating that most of the local moment is stabilized by the exchange energy from its own site. The difference of 0.033 Ry between these two values can then be attributed to interatomic exchange and arises from the exchange of the localized function Π_{3d} on A and the itinerant parts of the $3d$ electrons on other sites, primarily the nearest-neighbor atoms, these itinerant parts being constituted by the plane waves admixed to the tight-binding functions. This picture of magnetization formation by a strong intra-atomic exchange and alignment by interatomic exchange is similar to the conclusion drawn from earlier work in iron metal[1] and by Stearns[37] on the origin of ferromagnetism in transition metals. Although this is admittedly not a rigorous picture, we shall nevertheless, use here this interatomic exchange in the Heisenberg model[38] and make estimates of the spin-wave spectrum and the critical temperature. A more rigorous calculation of the critical temperature, in cobalt metal, using the vertex part procedure[39] appropriate for the itinerant picture will be reported in a separate article.[40] For the Heisenberg model we need an estimate of the nearest-neighbor exchange integral J. Assuming that the localized part of the spin arises from 1.471 unpaired electrons obtained from the difference of the localized spin populations in the last two rows of the second column in Table IV, one has a net spin of $S=0.736$ at each atomic site. Considering that there are 12 nearest neighbors at almost equal distances since c/a is close to ideal, the exchange between pairs of nearest neighbors per localized $3d$ electron is $J=0.0330/1.471\times 12$ Ry $=0.001\,87$ Ry, which occurs in the Hamiltonian in the Heisenberg model:

$$\mathcal{H} = -2J\sum_{i>j}\vec{S}_i\cdot\vec{S}_i - g\beta H\sum_i S_{iz}. \tag{5.1}$$

The resulting spin-wave spectrum[41] for hcp structure is given by:

$$\hbar\omega = (8D/c^2)(1-\cos\tfrac{1}{2}q_c) \tag{5.2}$$

for spin waves with wave vectors in z direction, c being the usual real space lattice constant in the z direction. The value of D is given by $1.15JSc^2$. Using our estimates of J and S we get $D=462$ meV Å^2 in good agreement with the experimental value[42] of $D=437\pm 20$ meV Å^2. This agreement indicates that at least as far as spin waves are concerned, the picture of $3d$ electrons as essentially localized, with the itinerant parts helping to provide the interatomic exchanges is essentially correct. The ratio between the 1.471 local unpaired $3d$ electrons per atomic site and the net 1.543 unpaired $3d$ band electrons per site indicates 95% localization of the magnetization with 5% itinerancy. Also, using the theory of Rushbrooke and Wood,[43] we can estimate the critical temperature T_c based on this localized spin interatomic exchange model. For an fcc lattice, which is very close to the hcp lattice, for the ideal c/a ratio, they find

$$\theta_c = (z-1)(0.578X - 0.0651), \tag{5.3}$$

where $\theta_c = k_B T_c/J$; $X=S(S+1)$, and z is the coordination number, which is 12 for both fcc and hcp structures. Using $J=0.001\,87$ Ry and $S=0.736$, we obtain $T_c=2184$ °K. The experimental value[38] is 1395 °K. The difference in the two values of T_c is reasonable considering the approximate nature of the Heisenberg model and the estimation of J in the present case.

It is worth commenting on the role played by Hubbard correlation in determining the magnetic moment. The role of Hubbard correlation[1] is mainly to reduce the splitting between the majority and minority $3d$ bands. Without it, the splitting would probably have been about 0.6 Ry rather than the present value of 0.29 Ry, and would have given a much larger magnetic moment (about $2.5\mu_B$ per atom). This result reconfirms the belief that in HF theory it is easier to obtain a ferromagnetic state than in a theory incorporating correlation, which shields the exchange. The Hartree-Fock limit is the wide band limit as can be seen from Eq. (3.5), by putting $\Delta\to\infty$. If we put $\Delta\to 0$ in Eq. (3.10), we get the most correlated $3d$ bands (the atomic limit) and the magnetization reduces to about $1.0\mu_B$ in the first cycle of self-consistency. The atomic limit is attained when there is no interatomic overlap, because, then the bandwidth can go to zero. In a thought experiment, we see that if the calculation is done for atomic separations larger than the actual, the bandwidth would be smaller, the Hubbard correlation stronger and so, starting the calculation with $1.56\mu_B$ per atom, the magnetization at the end of the first cycle will be smaller and successively decrease at each cycle settling at a

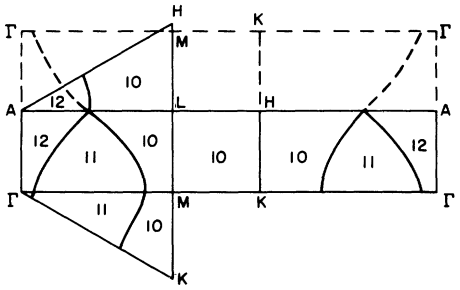

FIG. 10. Majority-spin Fermi-surface cross sections. Numbers represent the number of occupied bands in various parts of the Brillouin zone. Scale is 1 mm = 0.0352.

small value, which will tend to zero at infinite separation. This clearly shows the role of the itinerancy or the width of the $3d$ band in getting the self-consistent value of the magnetization. In summary then, this analysis of the spin-wave spectrum, Curie temperature, and the role of Hubbard correlation indicates that at low temperatures, the actual state of the system can be described as intermediate between the localized and itinerant pictures, being closer to the first, and it is very important to have the proper amount of correlation effects[19,21] on the electronic energies and wave functions to get the right value of the average magnetic moment per atom and its distribution in the metal.

C. Fermi-surface cross sections

From the intersections of the Fermi level with the energy bands in various directions we have drawn the majority-spin and minority-spin Fermi surface cross sections in some of the important planes. These are shown in Figs. 10 and 11. An estimate of the cross sections in these planes,

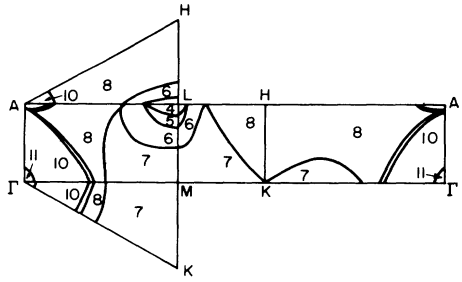

FIG. 11. Minority-spin Fermi-surface cross sections. Numbers represent the number of occupied bands in various parts of the Brillouin zone. Scale is 1 mm = 0.0352.

TABLE IX. Fermi-surface cross sections.[a]

Plane	Nature	Area (theor.)	Area (expt.)
Γ*MK*	majority elect.	0.014 ± 0.004	0.0095
Γ*MK*	majority elect.	1.096 ± 0.01	
Γ*ALM*	majority elect.	1.156 ± 0.01	
Γ*AHK*	majority elect.	1.135 ± 0.01	
Γ*MK*	minority elect.	0.314 ± 0.01	
Γ*MK*	minority elect.	0.358 ± 0.01	
Γ*MK*	minority elect.	0.512 ± 0.01	
Γ*MK*	minority elect.	0.006 ± 0.003	0.0028
ALH	minority elect.	0.044 ± 0.005	0.0315
ALH	minority hole	0.013 ± 0.005	
ALH	minority hole	0.066 ± 0.01	
Γ*ALM*	minority elect.	0.012 ± 0.004	0.0059
Γ*ALM*	minority elect.	0.299 ± 0.01	
Γ*ALM*	minority elect.	0.328 ± 0.01	
Γ*ALM*	minority elect.	0.014 ± 0.004	
Γ*ALM*	minority elect.	0.017 ± 0.004	0.0276
Γ*ALM*	minority hole	0.018 ± 0.04	
Γ*ALM*	minority hole	0.040 ± 0.05	0.0445
Γ*ALM*	minority hole	0.215 ± 0.01	
MKHL	minority hole	0.004 ± 0.002	0.0035
MKHL	minority hole	0.011 ± 0.004	
MKHL	minority hole	0.078 ± 0.01	
MKHL	minority elect.	0.265 ± 0.01	
Γ*AHK*	minority elect.	0.269 ± 0.01	
Γ*AHK*	minority elect.	0.340 ± 0.01	
Γ*AHK*	minority elect.	0.012 ± 0.004	
Γ*AHK*	minority elect.	0.014 ± 0.004	
Γ*AHK*	minority elect.	0.017 ± 0.004	
Γ*AHK*	minority hole	0.158 ± 0.01	

[a] The units are a_0^{-2}. A graphical representation of these cross sections is given in Fig. 10 for spin-up Fermi surface and in Fig. 11 for spin-down Fermi surface. The experimental values are from J. R. Anderson *et al.*, Ref. 7.

obtained from these figures, is given in Table IX. Experimental values are available for the small cross sections, from de Haas–van Alphen effect measurements in cobalt by Rosenman and Batallan,[6] and by Anderson, Hudak and Stone.[7] The minority-spin Fermi surface is very complicated because the Fermi level lies inside the $3d$ band. The numbers in the Figs. 10 and 11 refer to the total number of band electrons that are below the Fermi level at the particular point in the BZ. For majority spin we see just one Fermi surface which in the extended zone picutre, extends into the second zone with a large belly at the Γ*MK* plane and a small neck at another plane parallel to Γ*MK* at a distance of $2\pi/c$. For minority spin, we see four electron surfaces around the Γ point. The comparison between theory and the experimental values for the small cross sections is seen to be fairly good from Table IX.

D. Work function

Unlike the practice in usual earlier band-structure calculations, the present work as also the earlier calculation[1] on ferromagnetic iron, does not use an arbitrary zero of energy. The potentials in this work were always calculated with the potential of free space as the zero of energy. Thus our value of $\epsilon_F = -0.337$ Ry does have physical importance and should be compared with the negative of the work function. The experimental value[18] of the work function is 0.31 ± 0.015 Ry. Our value is a little larger in magnitude than the experimental result. The resolution of the small difference would require a consideration of collective effects involving the remaining electrons after the electron is emitted from the metal surface and the role of surface states which could make the work function for the surface different from the bulk metal.

E. Electron density of states

For the calculation of the density of states, the following procedure was adopted. A number of equally spaced energy levels from -1.2 to 0.00 Ry were chosen and for each of these energies, the number of states below each was obtained by a counting procedure in the Brillouin zone applying appropriate weight factors to the various sample points. The density of states was obtained by dividing the number of states in a particular energy interval by the energy interval. The density of states obtained in this way for any energy was averaged over a few energy intervals to remove any sharp discontinuities due to the discrete nature of the sample points in the BZ. Figure 6 shows the density of states for both the spin-up and down electron states separately and Fig. 7 the combined density of states. The width of the $3d$ part of the density of states is about 0.34 Ry for spin-up states and 0.34 Ry for spin-down states. The exchange splitting between the $3d$ bands is seen to be about 0.29 Ry. On the other hand, Wakoh and Yamashita's calculation[2] for a paramagnetic state needed a rigid band splitting of only 0.126 Ry to explain the right magnetic moment. Also, the bandwidth in their calculation is about 0.32 Ry. So, our bandwidth agrees fairly well with Wakoh and Yamashita's bandwidth. The exchange splitting obtained in Wakoh and Yamashita's calculation is however significantly smaller, owing to reasons explained earlier in this section.

The density of states at the Fermi states is somewhat difficult to obtain accurately, especially for the minority spins due to the sharp variations of $dn/d\epsilon$ at ϵ_F as seen from Fig. 6. The values we have obtained from our histograms are 1.9 per atom from majority spins and 15 per atom from minority spins. Thus the electronic contribution to the specific heat, given by

$$\gamma = (3\pi^2 k^2)^{-1} \left(\frac{dn^{\uparrow}}{d\epsilon} + \frac{dn^{\downarrow}}{d\epsilon} \right)_{\epsilon = \epsilon_F},$$

is 7.6×10^{-4} cal/mol °K^2. The experimental value[44] of γ is 11.3×10^{-4} cal/mol °K^2. The difference between the two values could be partly explained by the influence of electron-phonon interaction.[45]

The $3d$ density of states has a high peak at the high-energy end of the band and a low value at the low-energy end. This can be explained physically by the fact that in a given band, the lower-energy regions correspond to the states that have a larger admixture of plane waves in them. When the mixing of plane waves is weaker, the states are more atomic like, leading to the high peak at the high energy end. We may also mention here that from a quick look at the self-consistent density matrix sums given in Table IV, it is obvious that the electrons in the minority $3d$ bands hybridize more strongly with plane-wave states than do the electrons in the majority $3d$ bands. This is because the density of freelike states in the region occupied by the minority $3d$-band electrons is larger than that in the region of the majority $3d$ band. Considering now the total density of states from majority- and minority-spin electrons, we see that is has a sharp peak at 0.03 Ry below the Fermi level (ϵ_F) and a wide peak at 0.23 Ry below ϵ_F. Similar sets of two peaks have been obtained by Wakoh and Yamashita[2] and by Wohlfarth.[4] The latest experimental photoemission results[9] show only one asymmetric peak at 0.03 Ry below the Fermi level (ϵ_F), in agreement with our first peak. We would like to offer a possible explanation for the absence of the other peak in the experimental data. The experimental data measure a transition from an initial state to a final ionized state. Energy changes associated with the relaxation and correlation effects[46] in the final $3d$ hole state, which is fairly localized because the $3d$ bands are quite narrow, could move the 0.23 Ry peak towards the first peak resulting in the appearance of a single broad peak. Similar readjustments in inner levels following ionization of inner electrons have been observed in photoemission spectra.[10,46] This explanation needs to be explored more quantitatively.

VI. CONCLUSION

We have obtained the self-consistent Hartree-Fock electronic structure for hcp ferromagnetic

cobalt. The correlation effects on the energy level have been systematically included, in a practicable manner, for all the core $3d$-like states and freelike states, in the approximation of having electrons correlating in pairs. The success of the present calculation clearly indicates the feasibility and the usefulness of Hartree-Fock calculations in metals. This calculation is also the first one to include the core states along with the band states in Hartree-Fock band-structure calculations and the relations of results for these core states in the metal to pertinent properties of the metal, will be discussed in subsequent articles. Further, the treatment of the $3d$-band states in terms of nonoverlapping $3d$ atomic orbitals and plane waves has reduced the problem of the evaluation of the multicentered overlap integrals to only one-centered integrals, substantially reducing the computation time. This has made it possible for us to carry out some iterations for attaining self-consistency in the electronic structure.

The effect of the pair correlation on the energy levels was a lowering of different core and $3d$-like levels by different amounts. For band states, these energy shifts helped in producing the right values of the Fermi energy, the spin magnetic moment per atom, and good agreement in the Fermi-surface cross section with the ones obtained from experiment. The magnetization in the metal was found to arise mainly from the $3d$-like electrons. The magnetic moment and associated spin on each site was stabilized by intra-atomic exchange interactions while the alignment of spins was produced by the interatomic overlap and the exchange effects. An approximate analysis in the Heisenberg approximation of assuming localized spins on each site, with no itinerancy but still having an interatomic exchange, gave fairly good results for the spin-wave spectrum and the ferromagnetic critical temperature. In separate work,[40] we shall report the evaluation of the critical temperature based on an itinerant or band theory of phase transitions.

The present theory indicates two peaks in the total density of states, one peak near the Fermi energy coming from the minority-spin states and the other peak further away from the Fermi energy arising from the majority-spin states. Experimentally from photoemission measurements, only one peak near the Fermi energy is observed. A possible explanation that is suggested here is that in a ionized state that is localized, correlation effects among the remaining electrons are different[46] when the emitted $3d$ electron is from the majority- or minority-spin state, and, this could tend to combine the two peaks in the unionized system into one peak as explained in Sec. V, in the ionized case.

Finally, we would like to mention again that the effects of the electron-electron correlation in the partially filled minority $3d$ band are quite strong and their influence on the electronic energy bands and wave functions have been incorporated through the bandwidth-dependent Hubbard model. It would be desirable to attempt to incorporate these correlation effects in a more direct manner similar to the recent self-consistent perturbation approach[22] developed earlier for incorporation of many-body effects in metals.

ACKNOWLEDGMENT

The authors are very grateful to Dr. S. N. Ray for valuable discussions in the course of this work.

APPENDIX: PROCEDURE FOR EVALUATION OF COULOMB AND EXCHANGE MATRIX ELEMENTS

The process of simplification of Eqs. (2.34)–(2.36) for the Coulomb matrix elements and (2.37)–(2.39) for the exchange matrix elements to forms suitable for computation is rather complicated. We shall only outline the basic steps here and refer the reader elsewhere[23] for the complete expressions.

Thus, consider, as an example, one type of term, arising only from Eqs. (2.35) and (2.38) consisting of a matrix element in which all the four wave functions are tight binding in nature, namely,

$$\langle n_1 l_1 m_1 p_1 \vec{k}_1(\vec{r}_1); n_2 l_2 m_2 p_2 \vec{k}_2(\vec{r}_2)| \frac{2}{r_{12}} |n_3 l_3 m_3 p_3 \vec{k}_3(\vec{r}_1); n_4 l_4 m_4 p_4 \vec{k}_4(\vec{r}_2)\rangle$$

$$= \int\int d^3r_1\, d^3r_2\, \phi^*_{n_1 l_1 m_1 p_1, \vec{k}_1}(\vec{r}_1)\phi^*_{n_2 l_2 m_2 p_2, \vec{k}_2}(\vec{r}_2)\frac{2}{r_{12}}\phi_{n_3 l_3 m_3 p_3, \vec{k}_3}(\vec{r}_1)\phi_{n_4 l_4 m_4 p_4, \vec{k}_4}(\vec{r}_2) \quad \text{(A1)}$$

with the condition $\vec{k}_1 + \vec{k}_2 = \vec{k}_3 + \vec{k}_4$, this condition applying to all the six types of terms to be discussed here. Remembering that our tight-binding functions involve nonoverlapping atomic orbitals, we can express Eq. (A1) in the form:

$$\langle n_1 l_1 m_1 p_1 \vec{k}_1(\vec{r}_1); n_2 l_2 m_2 p_2 \vec{k}_2(\vec{r}_2)| \frac{2}{r_{12}} |n_3 l_3 m_3 p_3 \vec{k}_3(\vec{r}_1); n_4 l_4 m_4 p_4 \vec{k}_4(\vec{r}_2)\rangle$$

$$= \frac{1}{2N}\sum_{\vec{R}_j} \int \frac{2}{r_{12}} d^3r_1 d^3r_2 \left[\tfrac{1}{2}(1 + p_1p_2p_3p_4)\, e^{i(\vec{k}_4-\vec{k}_2)\cdot\vec{R}_j} \phi^*_{n_1 l_1 m_1}(\vec{r}_1)\phi_{n_3 l_3 m_3}(\vec{r}_1)\phi^*_{n_2 l_2 m_2}(\vec{r}_2-\vec{R}_j)\phi_{n_4 l_4 m_4}(\vec{r}_2-\vec{R}_j)\right.$$

$$+\tfrac{1}{2}(p_2p_4)\, e^{i(\vec{k}_4-\vec{k}_2)\cdot(\vec{R}_j+\vec{\rho})} \phi^*_{n_1 l_1 m_1}(\vec{r}_1)\phi_{n_3 l_3 m_3}(\vec{r}_1)\phi^*_{n_2 l_2 m_2}(\vec{r}_2-\vec{R}_j-\vec{\rho})\phi_{n_4 l_4 m_4}(\vec{r}_2-\vec{R}_j-\vec{\rho})$$

$$\left.+\tfrac{1}{2}(p_1p_3)\, e^{-i(\vec{k}_4-\vec{k}_2)\cdot(\vec{R}_j+\vec{\rho})} \phi^*_{n_1 l_1 m_1}(\vec{r}_1)\phi_{n_3 l_3 m_3}(\vec{r}_1)\phi^*_{n_2 l_2 m_2}(\vec{r}_2+\vec{R}_j+\vec{\rho})\phi_{n_4 l_4 m_4}(\vec{r}_2+\vec{R}_j+\vec{\rho})\right]. \tag{A2}$$

The terms involving odd numbers of p_i factors do not appear as a consequence of zero interatomic overlaps. For the evaluation of the one- and two-center integrals in this situation, we use the one-[31] and two-center[32] expansions of $1/r_{12}$

$$\frac{1}{r_{12}} = \sum_{lm} \frac{4\pi}{2l+1} \frac{r_<^l}{r_>^{l+1}} Y^*_{lm}(\theta_1, \phi_1) Y_{lm}(\theta_2, \phi_2) \tag{A3}$$

and

$$\frac{1}{r_{12}} = \sum_{l,l_j,m} B_{l,l_j,m} \frac{r_1^l r_{2j}^{l_j}}{R_j^{l+l_j+1}} \sum_{\mu,\mu'} e^{-(\mu-\mu')\phi_j} d^l(\theta_j)_{\mu,m} d^{l_j}(\theta_j)_{\mu',m} Y^*_{l,\mu}(\theta_1, \phi_1) Y_{l_j,\mu'}(\theta_{2j}, \phi_{2j}), \tag{A4}$$

where $r_<$ and $r_>$ are the smaller and larger of r_1 and r_2 and in Eq. (A3) (r_1, θ_1, ϕ_1) and (r_2, θ_2, ϕ_2) refer to the same coordinate frame. On the other hand, in Eq. (A4), (r_1, θ_1, ϕ_1) refer to a coordinate frame at the origin, with respect to which the position (R_j, θ_j, ϕ_j) of the atom j is defined, and $(r_{2j}, \theta_{2j}, \phi_{2j})$ refer to a coordinate frame located at $\vec{R}_j$ with the coordinate axes parallel to the one at the origin. The constants $B_{l,l_j,m}$ are given by

$$B_{l,l_j,m} = \frac{(-1)^{l_j+m} 4\pi}{[(2l+1)(2l_j+1)]^{1/2}} \times \frac{(l+l_j)!}{[(l+m)!(l-m)!(l_j+m)!(l_j-m)!]^{1/2}}. \tag{A5}$$

The ranges of l and l_j in Eqs. (A3) and (A4) are from 0 to ∞ and in Eq. (A4), m varies from $-l_{\min}$ to $l_{\min}$ where $l_{\min}$ is the smaller of l and l_j. The two-center expansion in Eq. (A4) of $1/r_{12}$ is valid for $r_1 + r_{2j}$ less than R_j, which is satisfied in our case because of the nonoverlapping nature of the atomic orbitals we have used. The $d^l(\theta)_{\mu,m}$ refer to the rotation matrices.[33]

Other types of Coulomb and exchange terms that can be evaluated similarly as (A1), are of two types, namely those involving three tight-binding functions and one plane wave or two plane waves and two tight-binding functions coordinate $\vec{r}_1$ associated with one plane wave and one tight-binding function and coordinate $\vec{r}_2$ with the other plane wave and tight-binding functions. In both these cases, one has to use the spherical Bessel function expansion of plane wave, in addition to Eqs. (A3) and (A4).

The fourth type of term that occurs in the Coulomb and exchange matrix elements also involves two plane waves and two tight-binding functions, but now the two functions associated with coordinate $\vec{r}_1$ are plane waves, and the two with coordinate $\vec{r}_2$ are tight-binding functions. In this type of term and the next two types, we have some cases where one encounters divergence, namely, where the wave vectors appearing with density coming from plane-wave products for one or the other electron add to zero. We shall first consider the nondivergent cases. Matrix elements of this type appear in Eqs. (2.34), (2.35), and (2.39). A typical example is

$$\int d^3r_1 d^3r_2 \phi^{\mathrm{PW}*}_{\vec{k}_1+\vec{K}_1}(\vec{r}_1)\phi^*_{n_2 l_2 m_2 p_2, \vec{k}_2}(\vec{r}_2)\frac{2}{r_{12}}\phi^{\mathrm{PW}}_{\vec{k}_3+\vec{K}_3}(\vec{r}_1)\phi_{n_4 l_4 m_4 p_4, \vec{k}_4}(\vec{r}_2)$$

$$= \frac{2\times 4\pi}{|\vec{k}_1+\vec{K}_1-\vec{k}_3-\vec{K}_3|^2} \frac{1}{2N\Omega} \frac{1}{2}\left(e^{i(\vec{K}_1-\vec{K}_3)\cdot\vec{\rho}/2} + p_2p_4\, e^{-i(\vec{K}_1-\vec{K}_3)\cdot\vec{\rho}/2}\right)$$

$$\times \sum_{l_0} 4\pi(-i)^{l_0} Y_{l_0,m_4-m_2}(\vec{k}_1+\vec{K}_1-\vec{k}_3-\vec{K}_3)\langle l_2 m_2; l_0, m_4-m_2 | l_4, m_4\rangle \int \Pi_{n_2 l_2}(r)\Pi_{n_4 l_4}(r)\, j_{l_0}(|\vec{k}_1+\vec{K}_1-\vec{k}_3-\vec{K}_3|r)\, dr. \tag{A6}$$

This evaluation procedure can be used as long as

$$\vec{k}_1+\vec{K}_1\neq\vec{k}_3+\vec{K}_3, \tag{A7}$$

so that there is no divergence.

The fifth type of matrix element has three plane waves and one tight-binding function. It appears in Eqs. (2.34), (2.36), (2.37), and (2.39) and can be evaluated similarly as (A6).

The sixth type of matrix element is the one with four plane waves and appears in Eqs. (2.34) and (2.37) only. An example is

$$\int d^3r_1\,d^3r_2\,\phi^{\mathrm{PW}*}_{\vec{k}_1+\vec{K}_1}(\vec{r}_1)\phi^{\mathrm{PW}*}_{\vec{k}_2+\vec{K}_2}(\vec{r}_2)\frac{2}{r_{12}}\,\phi^{\mathrm{PW}}_{\vec{k}_3+\vec{K}_3}(\vec{r}_1)\phi^{\mathrm{PW}}_{\vec{k}_4+\vec{K}_4}(\vec{r}_2)\frac{2\times4\pi}{|\vec{k}_1+\vec{K}_1-\vec{k}_3-\vec{K}_3|^2}\,\frac{1}{2N\Omega}\,\delta_{\vec{K}_1+\vec{K}_2,\vec{K}_3+\vec{K}_4}\delta_{\vec{k}_1+\vec{k}_2,\vec{k}_3+\vec{k}_4}. \tag{A8}$$

Again this result can be used directly for the nondivergent case characterized by the condition (A7).

Considering the divergent cases, for example, Eq. (A6) with $\vec{k}_1+\vec{K}_1=\vec{k}_3+\vec{K}_3$, one can get the result in Eq. (A9) below by substituting the momentum equality condition prior to applying the expansion in (A3). Thus,

$$\int d^3r_1\,d^3r_2\,\frac{1}{2N\Omega}\,\phi_{n_2l_2m_2p_2,\vec{k}_2}(\vec{r}_2)\frac{2}{r_{12}}\,\phi_{n_4l_4m_4p_4,\vec{k}_2}(\vec{r}_2)$$

$$=\left(\int\phi^*_{n_2l_2m_2}(\vec{r}_2)\phi_{n_4l_2m_2}(\vec{r}_2)\,d^3r_2\right)\delta_{l_2l_4}\delta_{m_2m_4}\delta_{p_2p_4}\frac{\int(2/r)\,d^3r}{2N\Omega}-\frac{2\times4\pi}{12N\Omega}\,\delta_{l_2l_4}\delta_{m_2m_4}\delta_{p_2p_4}\int\phi^*_{n_2l_2m_2}(\vec{r}_2)\phi_{n_4l_2m_2}(\vec{r}_2)\,r_2^2\,d^3r_2. \tag{A9}$$

Similarly, the other divergent terms that are encountered from the fifth and sixth types of terms referred to earlier can be expressed as:

$$\int d^3r_1\,d^3r_2\,\frac{1}{2N\Omega}\,\phi^{\mathrm{PW}*}_{\vec{k}_2+\vec{K}_2}(\vec{r}_2)\frac{2}{r_{12}}\,\phi_{n_4l_4m_4p_4,\vec{k}_2}(\vec{r}_2)$$

$$=\frac{1}{2N\Omega}\left(\frac{1}{\sqrt{\Omega}}\int e^{-i(\vec{k}_2+\vec{K}_2)\cdot\vec{r}_2}\phi_{n_4l_4m_4}(\vec{r}_2)\,d^3r_2\right)\frac{1}{2}\left(e^{i\vec{K}_2\cdot\vec{\rho}/2}+p_4e^{-i\vec{K}_2\cdot\vec{\rho}/2}\right)\int\frac{2}{r}\,d^3r$$

$$-\frac{2\times4\pi}{12N\Omega}\,\frac{1}{2}\left(e^{i\vec{K}_2\cdot\vec{\rho}/2}+p_4e^{-i\vec{K}_4\cdot\vec{\rho}/2}\right)\frac{1}{\sqrt{\Omega}}\int r^2e^{-i(\vec{k}_2+\vec{K}_2)\cdot\vec{r}}\phi_{n_4l_4m_4}(\vec{r})\,d^3r \tag{A10}$$

and

$$\int d^3r_1\,d^3r_2\,\frac{1}{2N\Omega}\,\phi^{\mathrm{PW}*}_{\vec{k}_2+\vec{K}_2}(\vec{r}_2)\frac{2}{r_{12}}\,\phi^{\mathrm{PW}}_{\vec{k}_2+\vec{K}_4}(\vec{r}_2)$$

$$=\left(\int\frac{2}{r}\,d^3r\right)\frac{1}{2N\Omega}\,\delta_{\vec{K}_2,\vec{K}_4}-\frac{2\times4\pi}{12N\Omega}\,\frac{1}{\Omega}\cos[(\vec{K}_4-\vec{K}_2)\tfrac{1}{2}\vec{\rho}]\int_{\mathrm{WS\ cell}}r^2e^{i(\vec{K}_4-\vec{K}_2)\cdot\vec{r}}\,d^3r. \tag{A11}$$

As indicated in Eq. (A11), the last integral is restricted to a Wigner-Seitz cell. The integral $\int(2/r)\,d^3r$ appearing in Eqs. (A9)–(A11) extends over all space and is divergent but it is exactly the same as the one obtained in Eq. (2.26), while evaluating the diagonal plane-wave–plane-wave matrix elements of the nuclear Coulomb potential. It can be easily seen that if the diagonal plane-wave–plane-wave matrix elements of the electronic Coulomb potential in Eq. (2.34) are combined with the diagonal plane-wave–plane-wave matrix elements of the nuclear Coulomb potential, the divergent integrals will identically cancel because of charge neutrality,[1] leaving only the second terms on the right-hand sides of Eqs. (A9)–(A11), which are nondivergent. Similarly, we can combine the electronic Coulomb potential terms in Eqs. (2.35) with the nuclear Coulomb potential terms in Eq. (2.22). The cancellation of divergent terms in these cases would not be exact as in the case just considered and we write

$$\int\frac{2}{r}\,d^3r=\sum_{\vec{R}_j}\left(\int_{\vec{R}_j-\vec{\rho}/2}\frac{2}{r}\,d^3r+\int_{\vec{R}_j+\vec{\rho}/2}\frac{2}{r}\,d^3r\right), \tag{A12}$$

where the integrations on the right-hand side of

Eq. (A12) are performed over Wigner-Seitz cells around atomic sites $\vec{R}_j - \frac{1}{2}\vec{\rho}$ or $\vec{R}_j + \frac{1}{2}\vec{\rho}$ and the origin for $\vec{r}$ is at $-\frac{1}{2}\vec{\rho}$. In this case, on consistently keeping the lattice summations over the same set of neighbors in Eqs. (A12) and (2.22), the cell by cell charge neutrality would lead to quick convergence. The cancellation of the divergent terms in Eq. (2.36) follows in the same way as for the divergent terms in Eq. (2.35).

When evaluating the exchange matrix elements given in Eqs. (2.37) and (2.39), divergent cases also seem to appear, but this divergence is only an apparent one. Thus, on carrying out the integration[1] over the reduced wave vector $\vec{k}'$ in Eq. (2.32), referring to the occupied part of the Brillouin zone, the divergent term has the following form:

$$\int \frac{d^3k'}{|\vec{k}' + \vec{K}' - \vec{k} - \vec{K}|^2} .$$

Near the divergence point $\vec{k}' + \vec{K}' = \vec{k} + \vec{K}$, we can approximate this integral for a small volume $\frac{4}{3}\pi k_0^3$ around $\vec{k} + \vec{K}$ by

$$4\pi \int_0^{k_0} \frac{(k')^2\, dk'}{(k')^2} = 4\pi k_0 \qquad \text{(A13)}$$

and thus obtain a finite result which tends to zero as the radius of the sphere around $\vec{k} + \vec{K}$ is reduced to zero. In actual numerical work, we have used k_0 in the range $0.05a_0^{-1}$ to $0.1a_0^{-1}$ over different regions of the Brillouin zone depending on the volumes assigned to the sample points in the BZ.

---

*Supported by NSF.

[1] K. J. Duff and T. P. Das, Phys. Rev. B 3, 192 (1971), 3, 2294 (1971).

[2] S. Wakoh and J. Yamashita, J. Phys. Soc. Jpn. 19, 1342 (1964); 21, 1712 (1966); 28, 1151 (1970).

[3] J. Callaway and C. S. Wang, Phys. Rev. B 7, 1096 (1973); J. Langlinais and J. Callaway, *ibid.* B 5, 124 (1972); J. Callaway and H. M. Chang, *ibid.* B 1, 305 (1970).

[4] L. Hodges, H. Ehrenreich, and N. D. Lang, Phys. Rev. 152, 505 (1966); L. Hodges and H. Ehrenreich, J. Appl. Phys. 39, 1280 (1968); E. P. Wohlfarth, *ibid.* 41, 1905 (1970).

[5] J. W. D. Connolly, Phys. Rev. 159, 415 (1967); Int. J. Quant. Chem. 25, 257 (1968).

[6] I. Rosenman and F. Batallan, Phys. Rev. B 5, 1340 (1971).

[7] J. R. Anderson, J. J. Hudak, and D. R. Stone, AIP Conf. Proc. 5, 477 (1972); 10, 46 (1973).

[8] R. V. Coleman, R. C. Morris, and D. J. Sellmyer, Phys. Rev. B 8, 317 (1973).

[9] D. E. Eastman, J. Appl. Phys. 40, 1386 (1969); D. E. Eastman and W. F. Krolikowski, Phys. Rev. Lett. 21, 623 (1968); D. E. Eastman, J. Phys. (Paris) 32, C1–293 (1971).

[10] S. Hufner and G. K. Wertheim, Phys. Rev. B 7, 2333 (1973).

[11] C. S. Fadley and D. A. Shirley, Phys. Rev. Lett. 21, 980 (1968).

[12] R. M. Moon, Phys. Rev. 136, A195 (1964); G. G. Scott, Rev. Mod. Phys. 34, 102 (1962).

[13] M. Kawakami, T. Hihara, Y. Koi, and T. Wakiyama, J. Phys. Soc. Jpn. 33, 1591 (1972).

[14] A. M. Portis and A. C. Gossard, J. Appl. Phys. 31, 205S (1960); A. C. Gossard, and A. M. Portis, M. Rubinstein, and R. H. Lindquist, Phys. Rev. 138, A1415 (1965).

[15] P. C. Riedi and R. G. Scurlock, Phys. Lett. A 24, 42 (1967).

[16] Mary Beth Stearns, Phys. Rev. B 4, 4069 (1971), 4, 4081 (1971); B 6, 3326 (1972).

[17] S. D. Mahanti, Taesul Lee, and T. P. Das, Phys. Rev. A 9, 2238 (1974).

[18] D. E. Eastman, Phys. Rev. B 2, 1 (1970).

[19] T. Lee, N. C. Dutta, and T. P. Das, Phys. Rev. A 4, 1410 (1971); S. N. Ray, T. Lee, and T. P. Das, *ibid.* A 7, 1469 (1973).

[20] H. P. Kelly and A. Ron, Phys. Rev. A 2, 1261 (1970).

[21] J. Hubbard, Proc. R. Soc. (London) A 243, 336 (1957). See also J. Kanamori, Prog. Theor. Phys. 30, 2751 (1963).

[22] C. M. Singal and T. P. Das, Phys. Rev. B 8, 3675 (1973).

[23] C. M. Singal, Ph.D. thesis (State University of New York, Albany, New York, 1973) (unpublished), Chaps. 5–8.

[24] J. C. Slater, *Quantum Theory of Atomic Structure* (McGraw-Hill, New York, 1960), Vol. II.

[25] J. B. Mann, *Atomic Structure Calculations I.* (National Bureau of Standards, 1967, U. S. Dept. of Commerce No. 22151).

[26] C. Froese, Can. J. Phys. 41, 1895 (1963).

[27] See for example: R. E. Watson and A. J. Freeman, in *Hyperfine Interactions*, edited by A. J. Freeman and R. B. Fraenkel (Academic, New York, 1967); M. H. Cohen, D. A. Goodings, and V. Heine, Proc. Phys. Soc. (London) 73, 811 (1959); V. Heine, Phys. Rev. 107, 1002 (1957); K. J. Duff and T. P. Das, Phys. Rev. 168, 43 (1968).

[28] S. Muller, Ph. Dunner, and N. Schmitz-Prangne, Z. Angew Phys. 22, 403 (1967).

[29] W. A. Harrison, *Pseudopotential in the Theory of Metals* (Benjamin, New York, 1966).

[30] C. M. Singal, see Ref. 23.

[31] J. D. Jackson, *Classical Electrodynamics* (Wiley, New York, 1963).

[32] R. J. Buehler and J. O. Hirschfelder, Phys. Rev. 83, 628 (1951); J. O. Hirschfelder, C. F. Curtis, and R. B. Bird, *Molecular Theory of Gases and Liquids* (Wiley, New York, 1954).

[33] M. E. Rose, *Elementary Theory of Angular Momentum* (Wiley, New York, 1957); E. P. Wigner, *Group Theory* (Academic, New York, 1959).

[34] H. P. Kelly and A. Ron, Phys. Rev. A 4, 11 (1971). Since cobalt atom correlation energy diagram values are not available, we have used the results of iron atom. We do not except any significant differences based on a comparison of the iron correlation energy

diagrams with the corresponding diagrams for the adjacent Mn atom (Ref. 35).
[35]D. Ikenberry, S. N. Ray, T. Lee, and T. P. Das (unpublished).
[36]S. N. Ray, T. Lee, and T. P. Das, Phys. Rev. B 8, 5291 (1973).
[37]M. B. Stearns, Phys. Rev. B 8, 4383 (1973).
[38]J. C. Slater, *Theory of Molecules and Solids* (McGraw-Hill, New York, 1974), Chaps. 9 and 10.
[39]E. Telemann, G. Ciobanu, and A. B. Fazakas, Phys. Status Solidi B 52, 375 (1972).
[40]C. M. Singal, G. Ciobanu, and T. P. Das, Phys. Rev. B 12, 2808 (1975).
[41]G. G. Low, Proc. Phys. Soc. (London) 79, 473 (1962).
[42]Z. Dimitrijevic, S. Krasnicki, J. Todorovic, and A. Wanic, Physica 37, 501 (1967); H. A. Alperin, O. Steinsvoll, G. Shirane, and R. Nathans, J. Appl. Phys. 37, 1052 (1966).
[43]G. S. Rushbrooke and P. J. Wood, Proc. Phys. Soc. (London) A 71, 257 (1958).
[44]C. H. Cheng, C. T. Wei, and P. A. Beck, Phys. Rev. 120, 426 (1960).
[45]D. Pines, *Elementary Excitations in Solids* (Benjamin, New York, 1964).
[46]A. J. Freeman, P. S. Bagus, and J. V. Mallow, Int. J. Magnet. 4, 35 (1973); P. S. Bagus, A. J. Freeman, and F. Sasaki, Phys. Rev. Lett. 30, 850 (1973).